UNIVERSIDADE DE SÃO PAULO
INSTITUTO DE FÍSICA DE SÃO CARLOS

JOÃO CARLOS DE ANDRADE GETELINA

On the critical behavior of the XX spin-1/2 chain under correlated quenched disorder

São Carlos
2016

JOÃO CARLOS DE ANDRADE GETELINA

On the critical behavior of the XX spin-1/2 chain under correlated quenched disorder

Dissertation presented to the Graduate Program in Physics at the Instituto de Física de São Carlos, Universidade de São Paulo to obtain the degree of Master of Science.

Concentration area: Basic Physics
Advisor: Prof. Dr. José Abel Hoyos Neto

Corrected Version
(Original version available on the Program Unit)

São Carlos
2016

Cataloguing data reviewed by the Library and Information Service
of the IFSC, with information provided by the author

Getelina, João Carlos de Andrade
On the critical behavior of the XX spín-1/2 chain under correlated quenched disorder / João Carlos de Andrade Getelina; advisor José Abel Hoyos Neto - versão corrigida -- São Carlos 2016.
82 p.

(Master's degree - Graduate Program in Basic Physics) -- Instituto de Física de São Carlos, Universidade de São Paulo - Brasil , 2016.

1. Spin-1/2 chains. 2. Disordered systems. 3. Phase transitions. I. Hoyos Neto, José Abel, advisor. II. Title.

Acknowledgements

I would like to thank my advisor professor Dr. José Abel Hoyos Neto, our collaborator professor Dr. Francisco Castilho Alcaraz, and my friends Diego Alejandro Carvajal Jara and Matheus Oliveira Schossler. I also show my gratitude to IFSC for providing everything I needed for my work and to CAPES for the financial support.

Abstract

GETELINA, J. C. A. **On the critical behavior of the XX spin-1/2 chain under correlated quenched disorder**. 2016. 82 p. Dissertation (Master in Science) - Instituto de Física de São Carlos, Universidade de São Paulo, São Carlos, 2016.

This work provides a full description of the critical behavior of the XX spin-1/2 chain under correlated quenched disorder. Previous investigations have shown that the introduction of correlation between couplings in the random XX model gives rise to a novel critical behavior, where the infinite-randomness critical point of the uncorrelated case is replaced by a family of finite-disorder critical points that depends on the disorder strength. Here it is shown that most of the critical exponents of the XX model with correlated randomness are equal to clean (without disorder) chain values and do not depend on disorder strength, except the critical dynamical exponent and the anomalous dimension. The former increases monotonically with disorder strength, whereas the results obtained for the latter are unreliable. Furthermore, the scaling relations between the critical exponents were also tested and it was found that those involving the system dimensionality, namely the hyperscaling and Fisher's scaling relations, are not respected. Measurements of the Rényi entanglement entropy of the system at criticality have also been performed, and it is shown that the scaling behavior of the correlated-disorder case is similar to the theoretical prediction for the clean chain, displaying the same finite-size correction and a disorder-dependent effective central charge in the leading term of the scaling. Further corrections to the scaling of the entanglement entropy were also investigated, but the results are inconclusive. The model was studied via exact numerical diagonalization of the corresponding Hamiltonian.

Keywords: Spin-1/2 chains. Disordered systems. Phase transitions.

Resumo

GETELINA, J. C. A. **O comportamento crítico da cadeia XX de spin-1/2 sob desordem correlacionada e independente do tempo**. 2016. 82 p. Dissertação (Mestrado em Ciências) - Instituto de Física de São Carlos, Universidade de São Paulo, São Carlos, 2016.

Este trabalho proporciona uma descrição completa do comportamento crítico da cadeia XX de spin-1/2 sob desordem correlacionada e independente do tempo. Investigações prévias mostraram que a introdução de correlação entre os acoplamentos da cadeia XX desordenada ocasiona o aparecimento de um novo comportamento crítico, onde o ponto crítico de desordem infinita da cadeia não-correlacionada é substituído por uma família de pontos críticos com desordem finita que depende da intensidade da desordem. Mostra-se aqui que a maioria dos expoentes críticos da cadeia XX com desordem correlacionada são iguais aos valores da cadeia limpa (sem desordem) e não dependem da intensidade da desordem, com exceção do expoente dinâmico crítico e da dimensão anômala. O primeiro cresce monotonicamente com a intensidade da desordem, enquanto que para o segundo os resultados obtidos não são confiáveis. Além disso, as relações de escala entre os expoentes críticos também foram testadas, e encontrou-se que aquelas envolvendo a dimensionalidade do sistema, isto é as relações de hiperescala e de Fisher, não são respeitadas. Medidas da entropia de emaranhamento de Rényi do sistema na criticalidade também foram efetuadas, e mostra-se que o comportamento de escala do caso com desordem correlacionada é semelhante à previsão teórica para a cadeia limpa, exibindo a mesma correção de tamanho finito e uma carga central dependente da desordem no termo principal da função de escala. Correções adicionais à função de escala da entropia de emaranhamento também foram investigadas, mas os resultados são inconclusivos. O modelo foi estudado pela diagonalização numérica exata do Hamiltoniano correspondente.

Palavras-chave: Cadeias de spin-1/2. Sistemas desordenados. Transições de fase.

List of Figures

Figure 1 – Phase diagram of the XX model. The order parameter m is defined in Eq. 3.12. 20

Figure 2 – Schematic picture of the XX model under correlated disorder. 23

Figure 3 – Gap energy Δ vs. the chain size L for several disorder strengths D. For $D \leq 1.0$ it is also shown the gap for the uncorrelated (uncorr) case. The data points were averaged until its relative error was about 1%. The black dashed line corresponds to the clean system. The colored lines are guide to the eyes. 27

Figure 4 – Critical dynamical exponent z vs. disorder strength D. The exponent was fitted from the finite-size gap, as in Fig. 3, for two ranges of L varying as a power of two. The black dashed line represents the clean exponent value. 28

Figure 5 – Specific heat C vs. the temperature T for the clean chain ($D = 0$) at criticality for various chain sizes L. Inset: C vs. T for various disorder strengths D and lattice size $L = 2^{12}$, averaged over 10^4 disorder realizations. The lines are guide to the eyes. 29

Figure 6 – Comparison between the critical dynamical exponent z (red circles) and the thermodynamic exponents at criticality α_T and γ_T of the specific heat C and the magnetic susceptibility χ, respectively. The exponents are plotted vs. the disorder strength D. The thermodynamic exponents were fitted for every value of D from the data similar to the inset of Fig. 5, using the same temperature range and chain size $L = 2^{12}$. The critical dynamical exponent is a reproduction of Fig. 4. 29

Figure 7 – Average and typical (typ) spin-spin correlation function for various disorder strengths D and lattice size $L = 2^{10}$. Panels (a) and (b) show the x and z-components, respectively. The data were averaged over 10^3 disorder realizations. Some curves are overlapped with the black dashed line, which corresponds to the clean chain with size $L = 2^{12}$. 31

Figure 8 – Critical exponent a_α of the average and typical spin-spin correlation function vs. disorder strength D. Panels (a) and (b) correspond to $\alpha = x$ and $\alpha = z$, respectively. The exponents were fitted from the data of the correlation, as shown in Fig. 7, for chain size $L = 2^{10}$ and within the region $1 \ll r \ll L$. The black dashed line is the clean exponent value. The colored lines are guide to the eyes. 32

Figure 9 – Average and typical (typ) dimer-dimer correlation function for various disorder strengths D and chain size $L = 2^{10}$. The data were averaged over 10^4 disorder realizations. The black dashed line corresponds to the clean chain with size $L = 2^{12}$. 34

Figure 10 – Critical exponent a_{dd} of the average and typical dimer-dimer correlation function vs. disorder strength D. The exponents were fitted from the data of the correlation, as shown in Fig. 9, for lattice size $L = 2^{10}$ and within the region $1 \ll r \ll L$. The black dashed line is the clean exponent value. The colored lines are guide to the eyes. 34

Figure 11 – Gap energy Δ vs. distance from criticality θ for disorder strength $D = 0.1$ and $D = 1.0$ and chain sizes L. The samples were averaged until the relative error was about 1%. The black dashed line corresponds to the clean chain with $L = 4096$. The colored lines are guide to the eyes. . . . 36

Figure 12 – Gap energy Δ of the clean chain divided in two subsystem A and B of sizes l and $L - l$, respectively. The former has couplings $J_A = 0.1$, whereas the latter has couplings $J_B = 1.0$. The gap energy Δ is plotted as a function of l for various distances from criticality θ. The lines are guide to the eyes. Inset: Average minimum coupling J_{min} vs. the chain size L for three disorder strengths D, averaged over 10^5 disorder realizations. The black lines are the best fit with respective exponent a_D. 37

Figure 13 – Specific heat C' of the quantum phase transition vs. the distance from criticality θ for several disorder strength D and lattice size $L = 512$. The data were obtained from the differentiation of the ground-state energy E_0 with respect to θ. Each E_0 was averaged over 10^5 disorder realizations. The lines are guide to the eyes. 38

Figure 14 – Susceptibility χ vs. the distance from criticality θ for several disorder strengths D. Here the susceptibility is the sum of the dimer-dimer correlation function $G^{dd}(r)$ over the distance r. $G^{dd}(r)$ was computed for chain size $L = 512$ and averaged over 10^3 disorder realizations. The lines are guide to eyes. 39

Figure 15 – Dimer operator M_i vs. the position i for various disorder strenghts D. It was considered a single disorder realization, with chain size $L = 128$ and distance from criticality $\theta = e^{-3}$. The lines are guide to the eyes. . 40

Figure 16 – Dimer order parameter m vs. (a) the distance from criticality θ and (b) the conjugate field B for several disorder strengths D and chain size $L = 512$. The data were averaged over 10^5 disorder realizations. Colored lines are guide to the eyes. 41

Figure 17 – The x and z-components of the spin-spin correlation function for various distances from criticality θ and lattice size $L = 2^{11}$. The dot-dashed lines correspond to the clean chain, while the continuous ones correspond to $D = 1.0$. The data were averaged over 10 and 10^3 disorder realizations for the x and z-directions, respectively. 42
Figure 18 – Dimer-dimer correlation function $G^{dd}(r)$ for various distances from criticality θ and chain size $L = 2^{11}$. The dot-dashed lines correspond to the clean chain, while the continuous ones correspond to $D = 1.0$. The data were averaged over 10^4 disorder realizations. 43
Figure 19 – Scaling of the x and z-component spin-spin correlation functions for various distances from criticality θ and disorder strengths D. The input exponent values a_x and a_z are shown in Table 2. 45
Figure 20 – Scaling of the dimer-dimer correlation function G^{dd} for various distances from criticality θ and disorder strengths D. The input exponent values a_{dd} are shown in Table 2. 46
Figure 21 – Critical exponent η vs. the disorder strength D. The dashed line gives the clean chain exponent value. The red line is a guide to the eye. . . . 47
Figure 22 – Schematic of two spins i and j in a periodic spin chain of size L connected by the chord length (dashed line). 50
Figure 23 – Scaling function of the Rényi entanglement entropy $S_n(x)$ for $n = 1$ (black points) and $n = 2$ (red points), using $c = 1.20$ as the input central charge. The data were calculated for disorder strength $D = 1.0$ and chain size $L = 2^{10}$, averaging over 10^5 disorder realizations. The green line represents the expected scaling. 52
Figure 24 – Rényi entanglement entropy $S_n(x)$ for various n and two disorder strengths D, namely and chain sizes $L = 200$ and $L = 400$ for disorder strength $D = 1.0$ (top panel) and $D = 2.0$ (bottom panel). The data were averaged over 10^3 disorder realizations. The lines are guide to the eyes. 53
Figure 25 – Central charge c vs. disorder strength D fitted from the von Neumann entanglement entropy $S_1(x)$. The entanglement entropy was calculated for two chains with size $L = 200$ (blue triangles) and $L = 400$ (red circles), averaging over 10^3 disorder realizations for each value of D. The black dashed line is the clean chain central charge. Colored lines are guide to the eyes. 54
Figure 26 – The parameters a_0 and a_2 (see Eq. 4.9) vs. n (panels (a) and (b), respectively) for various disorder strengths D. The parameters were fitted from the average entanglement entropy $S_n(x)$, which was calculated for chain size $L = 1024$. 55

Figure 27 – Central charge c vs. the parameter n for disorder strength $D = 0.1$ (panel (a)) and $D = 1.0$ (panel (b)). The central charge was fitted from the average entanglement entropy $S_n(x)$, which was calculated for various chain sizes L. The dashed line in panel (a) is the clean chain central charge. 56
Figure 28 – Central charge c vs. the parameter n for disorder strength $D = 2.0$. The central charge was fitted from the average entanglement entropy $S_n(x)$, which was calculated for various chain sizes L. 57
Figure 29 – The exponent ϕ vs. the parameter n for disorder strengths $D = 0.1$ and $D = 1.0$. The exponent was fitted from the average entanglement entropy $S_n(x)$, which was calculated for various chain sizes L. The dashed line is the clean chain exponent. 57
Figure 30 – Rényi entanglement entropy $S_n(x)$ for various n, disorder strength $D = 1.0$ and lattice size $L = 1024$. The data were averaged over 10^3 disorder realizations. The dashed lines were calculated from Eq. 4.11 using the best fitting values of the parameters. 58
Figure 31 – Relative error σ_i vs. the eigenvalue λ_i for (a) various chain size L and disorder strength $D = 5.0$ and (b) several disorder strengths and chain size $L = 2^{10}$. The eigenvalues were averaged over 10^3 disorder realizations. Eigenvalues calculated from H and H^2 are represented as filled and open symbols, respectively. The dashed line delimits the desired precision. Colored lines are guide to the eyes. 72

Contents

1 INTRODUCTION 15

2 THE XX MODEL 17
2.1 Mapping to free fermions 17
2.2 The dimer phase transition and the effects of disorder 19
2.3 The correlated disorder case 22

3 CRITICAL EXPONENTS OF THE XX MODEL WITH CORRELATED DISORDER 25
3.1 Exponents at criticality 25
3.1.1 Dynamical and thermodynamic exponents 26
3.1.2 Spin-spin and dimer-dimer correlation functions 30
3.2 Exponents at the dimer phase (out of criticality) 33
3.2.1 Thermodynamic exponents 35
3.2.2 Spin-spin and dimer-dimer correlation functions 41

4 ENTANGLEMENT PROPERTIES OF THE XX MODEL WITH CORRELATED DISORDER 49
4.1 Scaling function and the central charge 49
4.2 Higher-order corrections of the scaling 53

5 CONCLUSION 59

REFERENCES 61

APPENDIX A – SOME PROPERTIES OF THE HAMILTONIAN . 67

APPENDIX B – NUMERICAL INSTABILITIES 71

APPENDIX C – EXPRESSIONS FOR THE SPECIFIC HEAT AND THE MAGNETIC SUSCEPTIBILITY 73

APPENDIX D – SPIN-SPIN AND DIMER-DIMER CORRELATION FUNCTIONS 77

APPENDIX E – FITTING METHOD OF THE ENTANGLEMENT ENTROPY SCALING WITH SUBLEADING TERMS 81

1 Introduction

Most of the research in theoretical condensed matter physics is concerned about the elaboration and solution of homogeneous (clean) models, mainly because these models are easier to solve and may even have an analytical solution. However, an idealized clean system does not describe quite well how real matter is. Materials usually have impurities or defects randomly distributed throughout them, i.e. they are disordered. (1–3) The study of disordered models came into prominence recently, thanks to the advance in computer simulations and the development of new mathematical techniques, such as the renormalization group. (4–6) Clean models are now being compared to their disordered counterpart to investigate how the introduction of disorder may affect the system behavior.

One example of such model is the XX spin-1/2 chain, which consists of a one-dimensional (1D) lattice of interacting spins whose x and y components are coupled. For the clean version of the XX model all those couplings are equal to the same constant, whereas for the disordered version they are realizations of a random variable with a given probability distribution. As a critical system, the XX model is fully described by its set of critical exponents. Research shows that the introduction of any amount of disorder completely changes the critical behavior of the XX model. (7)

Recently, a new configuration for the disordered XX model was proposed. (8) In this special setup, called here as the XX_{CD} model, the random couplings J_i are correlated, such that the odd couplings are equal to their first right neighbor, i.e. $J_{2i-1} = J_{2i}$. At first glance one could infer that this change would not affect the system properties, since from a macroscopic perspective the model is unaltered. However, it has been shown that the XX_{CD} model behaves in a unique way: Some of its critical exponents depend on how strong the disorder is, being equal to the clean value for weak disorder and exhibiting novel critical behaviors as disorder gets stronger. (9) This unusual behavior motivates a detailed study about the XX_{CD} model. Until now only a few properties of this system have been evaluated; a complete description of its critical behavior is still lacking.

The XX model displays a so-called quantum critical behavior, i.e. it undergoes a quantum phase transition (QPT). (10–14) QPTs are phase transitions driven by quantum fluctuations alone; they occur at zero temperature ($T = 0$). Thus, one could infer that the interest in QPTs is just theoretical. However, it has been observed experimentally systems with quantum critical behavior. (15–17) To observe this behavior one should consider sufficiently low temperatures, such that the thermal fluctuations are less significant than the quantum ones, i.e. $kT \lesssim \hbar\omega_C$, where ω_C is the characteristic frequency of the system.

The difference between classical and quantum phase transitions is that the latter does not allow temperature as a control parameter; all known properties of CPTs are extended to QPTs, such as the classification in first-order and continuous phase transitions, scale invariance, universality classes, etc. (For more details on CPTs see (18–20).) The similarities between quantum and classical phase transitions have been reinforced after the development of the quantum-to-classical mapping, which transforms a d-dimensional quantum critical system in a $(d+1)$-dimensional classical one. (12, 21) This mathematical trick consists of inserting an extra imaginary time dimension, which is represented as infinite copies of the original system. Using this technique one can, for instance, map a single quantum spin (with dimension $d = 0$) into a classical 1D Ising model.

Since the temperature T is not a possible control parameter for QPTs, these transitions are usually tuned by the parameters that appear in the Hamiltonian of the system. For spin chains, for example, such parameters are the couplings between spins or the external magnetic field. Therefore, to introduce disorder in a spin chain model one must make the couplings or the external field random. The former case is known as random-T_C disorder (or random mass in analogy with field theory), while the latter is known as random field disorder. (22) Randomness can be further classified according to its relation with the typical time scale of measurements: If disorder is time independent it is known as quenched disorder (i.e. frozen), whereas if it depends on time it is called as annealed disorder. In general, quenched disorder is more interesting than annealed disorder, because the effects of randomness are enhanced.

The XX model under uncorrelated quenched disorder has already been fully described. (23) Conversely, for the XX_{CD} model there are not many results available. First investigations, though, show that the introduction of correlated quenched disorder gives rise to novel critical behavior. Besides the theoretical interest in describing the XX_{CD} model, recent investigations have shown that a similar correlated-random model describes the behavior of a polymer with high conductivity. (24–26)

What follows in the next chapters is a complete description of the critical behavior of the XX_{CD} model, by determining the full set of critical exponents and checking the so-called scaling relations that connect these exponents with each other. Furthermore, entanglement properties of the XX_{CD} model are also studied. The results are compared to the theoretical predictions of the clean chain.

The remainder of this text is organized as follows. Chapter 2 presents the model and the method used for solving it, besides providing a discussion about the effects of disorder on the phase transition. In Chapter 3 the quantities of interest are evaluated and their corresponding critical exponents are determined. Chapter 4 shows the entanglement measurements, which is a trending topic in condensed matter physics. Concluding remarks are reported in Chapter 5.

2 The XX model

This chapter gives a discussion about the general properties of the XX model. In the first section the Hamiltonian is introduced, followed by an outline of the Jordan-Wigner transformation, which maps the interacting spin problem to a free fermion one. The second section presents the condition for criticality and the phases of the XX model. A derivation of the so-called Harris criterion is also presented, which determines whether weak disorder is perturbatively relevant for the critical behavior. The last section finally introduces the Hamiltonian of the XX_{CD} model in the appropriate basis. There is also a comment about a mathematical trick that yields faster calculations.

2.1 Mapping to free fermions

The general Hamiltonian of the 1D XX spin-1/2 chain with nearest neighbor interactions is

$$H_{XX} = \sum_{i=1}^{L} J_i \left(S_i^x S_{i+1}^x + S_i^y S_{i+1}^y \right), \tag{2.1}$$

where $J_i > 0$ are the couplings, S_i^α are the usual spin-1/2 operators* and L is the system size which shall be considered always even. For the clean chain the couplings are constant (i.e. $J_i = J$), whereas for the disorder chain the couplings J_i are realizations of a random variable.

The subject of this work is the so-called XX_{CD} model, where the couplings are random and also correlated with each other. To introduce this correlation between couplings, the odd sublattice couplings (i.e. J_{2i-1}) are randomly generated and the even sublattice ones are defined as equal to their left neighbor, i.e. $J_{2i} = J_{2i-1}$. Thus, the Hamiltonian of the XX_{CD} model can be written as

$$H = \sum_{i=1}^{\frac{L}{2}} J_i \left(S_{2i-1}^x S_{2i}^x + S_{2i-1}^y S_{2i}^y + S_{2i}^x S_{2i+1}^x + S_{2i}^y S_{2i+1}^y \right). \tag{2.2}$$

However, before giving further details about this model, in this section it is considered the Hamiltonian as in Eq. 2.1 to show some general properties of the XX model that are valid independently of the couplings nature.

*Throughout this paper it is considered that $\hbar = 1$ and $k = 1$, where $\hbar$ is the Planck constant over 2π and k is the Boltzmann constant.

Rewriting Eq. 2.1 with the raising and lowering operators $S_i^{\pm} \equiv S_i^x \pm iS_i^y$ gives

$$H_{XX} = \frac{1}{2}\sum_{i=1}^{L} J_i \left(S_i^+ S_{i+1}^- + h.c.\right). \tag{2.3}$$

To solve the Hamiltonian above one can transform $S_i^{\pm}$ into fermionic creation and annihilation operators $c_i^\dagger$ and c_i, respectively. (27) Such operators respect the following anti-commutation relations

$$\{c_i, c_j\} = \left\{c_i^\dagger, c_j^\dagger\right\} = 0, \tag{2.4}$$

$$\left\{c_i, c_j^\dagger\right\} = \delta_{i,j}, \tag{2.5}$$

and are defined as

$$c_i^\dagger \equiv S_i^+ \exp\left(\sum_{j=1}^{i-1} -i\pi S_j^+ S_j^-\right), \tag{2.6}$$

$$c_i \equiv \exp\left(\sum_{j=1}^{i-1} i\pi S_j^+ S_j^-\right) S_i^-. \tag{2.7}$$

This change of basis is known as the Jordan-Wigner transformation. Notice that it preserves the form of Eq. 2.3, since $c_i^\dagger c_j = S_i^+ S_j^-$, except for the last term in the summation, which depends on the boundary conditions. Considering a cyclic chain, i.e. $S_{L+1}^{\pm} = S_1^{\pm}$, and using Eq. 2.6 and Eq. 2.7 one finds

$$\begin{aligned} S_L^+ S_1^- &= c_L^\dagger \exp\left(\sum_{j=1}^{L-1} i\pi c_j^\dagger c_j\right) c_1, \\ &= \exp\left(\sum_{j=1}^{L} i\pi c_j^\dagger c_j\right) \exp\left(-i\pi c_L^\dagger c_L\right) c_L^\dagger c_1, \\ &= (-1)^{N+1} c_L^\dagger c_1, \end{aligned} \tag{2.8}$$

where $N = \sum_{i=1}^{L} c_i^\dagger c_i$ is the total number operator.

Thus, the transformed Hamiltonian with periodic boundary conditions is

$$H_{XX} = \frac{1}{2}\left[\sum_{i=1}^{L-1} J_i \left(c_i^\dagger c_{i+1} + h.c.\right) + (-1)^{N+1} J_L \left(c_L^\dagger c_1 + h.c.\right)\right]. \tag{2.9}$$

This is the free fermion representation of the XX model. The spins are now represented by fermionic particles hopping in the lattice with a energy cost equal to the coupling. The mapping between spins and fermions is given by

$$S_i^z = c_i^\dagger c_i - \frac{1}{2}. \tag{2.10}$$

Therefore, according to Eq. 2.10, if the action of the number operator $c_i^\dagger c_i$ in the i-th site gives one, there is a spin up in the z-direction in that site ($\langle S_i^z \rangle = 1/2$), while if the result is zero there is a spin down ($\langle S_i^z \rangle = -1/2$).

The problem now is to find the eigenvalues and eigenvectors of Eq. 2.9. For the clean case ($J_i = J$) this can be done exactly via a Fourier transform on the fermionic operators in Eq. 2.9, whereas the disordered case requires a numerical routine. The advantage of the free fermion representation for the disordered model is that it reduces significantly the size of the matrix to be diagonalized — from a $2^L \times 2^L$ to a $L \times L$ matrix — and, therefore, requires much less computational effort.

Nevertheless, there are some interesting properties of the Hamiltonian that are regardless of the couplings nature. For instance, as it is shown in Appendix A, the spectrum of H is symmetric, i.e. there are $L/2$ positive and negative eigenvalues (recall that L is always even) such that $\lambda_i = -\lambda_{L+1-i}$, where λ_i is the i-th eigenvalue and the spectrum is in ascending order ($\lambda_1 < \lambda_2 < \cdots < \lambda_L$).

The ground state $|GS\rangle$ is obtained by filling the vacuum $|0\rangle$ with quasiparticles whose energy is below the Fermi level, which is $\mu = 0$. Therefore, since half of the eigenvalues are negative, the ground state is

$$|GS\rangle = \prod_{i=1}^{L/2} \eta_i^\dagger |0\rangle , \tag{2.11}$$

where $\eta_i^\dagger$ is the i-th fermionic creation operator in the momentum space (see Appendix A). The ground-state energy E_0 is equal to the sum of all negative eigenvalues, i.e. $E_0 = \sum_{i=1}^{\frac{L}{2}} \lambda_i$. Furthermore, it is shown in Appendix A that $\langle GS| c_i^\dagger c_i |GS\rangle = \left\langle c_i^\dagger c_i \right\rangle = 1/2$, which yields $\langle S_i^z \rangle = 0$. The spin average for the other directions is also zero, because S_i^x and S_i^y are written as linear combinations of $S_i^\pm$ and $\left\langle S_i^\pm \right\rangle = 0$, since these operators do not preserve the number of particles. Thus, there is no magnetization in the ground state of the XX model, even though the temperature is zero. Those spin fluctuations are, thereby, caused uniquely by quantum effects.

2.2 The dimer phase transition and the effects of disorder

The seminal work that provided the solution of the XX model by mapping to free fermions also shows that the spin-spin correlation function scales as a power law. (27) The power-law scaling of the correlation function is a signature of a critical system. Thus, this result indicate that the XX model is critical. Indeed, the condition for criticality is guaranteed whenever (28)

$$\prod_{i=1}^{\frac{L}{2}} J_{2i-1} = \prod_{i=1}^{\frac{L}{2}} J_{2i}. \tag{2.12}$$

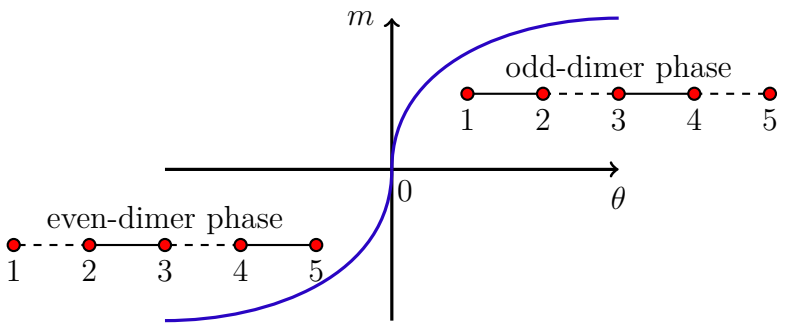

Figure 1 – Phase diagram of the XX model. The order parameter m is defined in Eq. 3.12.

Source: By the author.

It is clear that this criterion is fulfilled for the clean chain and for the XX_{CD} model, since the former has constant coupling and the latter has $J_{2i} = J_{2i-1}$. Conversely, for the uncorrelated random chain one can choose a probability distribution that still satisfies Eq. 2.12.

Using Eq. 2.12 one can define the distance from criticality as

$$\theta = \ln\left[\frac{\left(\prod_{i=1}^{\frac{L}{2}} J_{2i-1}\right)}{\left(\prod_{i=1}^{\frac{L}{2}} J_{2i}\right)}\right]. \tag{2.13}$$

According to Eq. 2.13, the system is driven out of criticality if the values of the odd or even couplings are changed. Multiplying the even couplings by a constant a, Eq. 2.12 gives, for the clean chain and for the XX_{CD} model,

$$\theta \;=\; \ln(a)\,. \tag{2.14}$$

For $a \to 0$ the even couplings vanish, yielding the formation of dimers in the odd sublattice. Similarly, if $a \gg 1$ the interactions from the odd sublattice are negligible, which results in dimers in the even sublattice (see the phase diagram in Fig. 1.). Hence, there are two ordered phases in the phase diagram of the XX model which are called as the odd-dimer and even-dimer phases. The critical exponents can be found in either of the ordered phases for θ close to zero. Thus, expanding Eq. 2.14 for a close to one gives

$$\theta \approx 1 - a. \tag{2.15}$$

Here it is chosen the odd-dimer phase to make the measurements, i.e. $a < 1$.

With the distance from criticality defined, one can now ask about the effects of disorder under the phase transition (PT) of the XX model. The most fundamental question would be if the PT occurs at all after introducing randomness. It has been already shown that disordered systems can indeed undergo a PT, but in early studies it was believed that randomness would eventually destroy the transition. To understand this concern, let the

uncorrelated random XX chain be divided in subsystems of equal size. Since the couplings are random, each subsystem could have its own distance from criticality θ and it was not known how to evaluate θ for the bulk system. This is the reason why random couplings are known as the random-T_C disorder.

This same argument, however, was used later to deduce a criterion that determines whether disorder is relevant to the PT of a system, as it is shown in the following. Suppose that a d-dimensional spin chain has a bulk nonzero θ and a corresponding correlation length ξ. This chain is divided in n subsystems of size ξ^d. One can calculate the average distance from criticality $\overline{\theta}$ and also its standard deviation $\Delta\theta$. According to the central limit theorem, the standard deviation scales as $\Delta\theta \sim \xi^{\frac{-d}{2}}$. Dividing this relation by $\overline{\theta}$ and using that $\xi \sim \theta^{-\nu}$, where ν is the clean correlation length exponent, one finds

$$\frac{\Delta\theta}{\overline{\theta}} \sim \xi^{\frac{-d}{2}+\frac{1}{\nu}}. \tag{2.16}$$

For consistency of the clean criticality, $\Delta\theta/\theta \to 0$. This is satisfied if the exponent on the right-hand side of Eq. 2.16 is negative, since $\xi \to \infty$ at the critical point. Hence,

$$d\nu > 2. \tag{2.17}$$

The expression above is known as the Harris criterion (12, 29, 30), and it gives a necessary but not sufficient condition for preserving the clean critical behavior of a system under the influence of disorder. When Eq. 2.17 is not fulfilled, disorder becomes relevant and a new critical behavior emerges. There are two known possibilities for this new behavior, namely the finite-disorder critical point (FDCP) and the infinite-randomness critical point (IRCP). The former changes the universality class of the clean critical point (CCP), yielding new critical exponent values. Conversely, the difference between the IRCP and the CCP is more significant: The usual power-law scaling of some quantities is replaced with an exponential scaling, i.e. the scaling becomes activated. An example of such activated scaling in the IRCP is the relation between the relaxation time and the correlation length. (12)

Notice that any amount of disorder affects the PT of the XX model, since $d\nu = 1$. Indeed, it was observed that under uncorrelated disorder this system exhibit the so-called activated scaling, which is a characteristic of the IRCP. (5, 23) Another property of those random critical points is that the observables are not self-averaging at criticality. (31–34) This means that the width of an observable distribution either stays constant (FDCP) or increases (IRCP) under coarse-graining, i.e. as L gets bigger. The consequence of non-self-averaging quantities is requirement of more disorder realizations as the lattice size increases.

The surprising result of the XX_{CD} model is that the CCP is preserved for weak disorder, even though the Harris criterion is not fulfilled. The criterion, however, should be

rewritten to consider the correlation between couplings. Assuming that there is a spatial correlation between the couplings J_i and J_j that decays with the distance $r = |j - i|$ as a power law with exponent $b > 0$, Eq. 2.17 is thus rewritten as (35)

$$\min\{d, b\}\,\nu > 2. \tag{2.18}$$

Nonetheless, for the case studied here the correlation is irrelevant to the criterion, since to obtain J_{2i-1} correlated only with its right neighbor one must have $b \to \infty$.

This contradiction between the Harris criterion and the behavior observed for the XX_{CD} model does not indicate that the former is wrong. Rather, the criterion is not applicable to the XX_{CD} model because of the way it is constructed. Making $J_{2i} = J_{2i-1}$ removes the random-T_C property of the system, which was the starting point in the deduction of Eq. 2.17. Therefore, using the Harris criterion to evaluate the XX_{CD} model is a fallacy. Furthermore, other apparent violations of the Harris criterion have already been reported. (36)

2.3 The correlated disorder case

The Hamiltonian of the XX_{CD} model in the free fermion basis with periodic boundary conditions is

$$H = \sum_{i=1}^{\frac{L}{2}-1} \left[J_i \left(c_{2i-1}^{\dagger} c_{2i} + a c_{2i}^{\dagger} c_{2i+1} + h.c.\right)\right] + J_{\frac{L}{2}} \left[\left(c_{L-1}^{\dagger} c_L + h.c.\right) + a\,(-1)^{N+1} \left(c_L^{\dagger} c_1 + h.c.\right)\right], \tag{2.19}$$

or in the matrix form

$$H = \begin{pmatrix} 0 & J_1 & 0 & \cdots & 0 & (-1)^{N+1} a J_{\frac{L}{2}} \\ J_1 & 0 & aJ_1 & \cdots & 0 & 0 \\ 0 & aJ_1 & 0 & \ddots & \vdots & \vdots \\ \vdots & \vdots & \vdots & \ddots & & \\ 0 & 0 & \cdots & & 0 & J_{\frac{L}{2}} \\ (-1)^{N+1} a J_{\frac{L}{2}} & 0 & \cdots & & J_{\frac{L}{2}} & 0 \end{pmatrix}. \tag{2.20}$$

This chain is depicted in Fig. 2. The couplings J_i are generated by a pseudo-random numerical routine with a uniform distribution bounded between zero and one. The default distribution can be modified by taking the D-th power of the given random number, which yields a new parameterized probability density function

$$P(J) = \frac{1}{D} J^{\frac{1}{D}-1}, \tag{2.21}$$

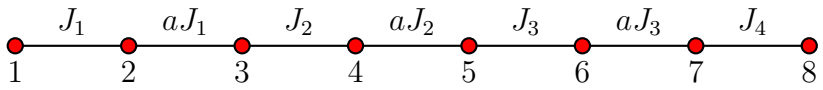

Figure 2 – Schematic picture of the XX model under correlated disorder.

Source: By the author.

where D is the so-called disorder strength.

Using Eq. 2.21 one can show that the ratio between the standard deviation σ_J and the average $\langle J \rangle$ of the couplings is

$$\frac{\sigma_J}{\langle J \rangle} = \frac{D}{\sqrt{2D+1}}. \tag{2.22}$$

Since the ratio $\sigma_J / \langle J \rangle$ increases monotonically with D, this definition of disorder strength is a reasonable one. Such definition, though, is not unique. One could choose, for instance, a truncated Gaussian distribution with fixed average and define disorder strength as the variation of the standard deviation. The distribution in Eq. 2.21 is preferred because it allows to investigate the effects of relatively strong disorder. Besides, it gives smooth curves for the critical exponents as a function of D, as shown in the next chapter.

For disordered systems each observable must be averaged over various disorder realizations. To obtain a reliable statistics, it is considered here at least 10^3 disorder realizations. Each one of them represents a unique Hamiltonian with a given set of couplings. The Hamiltonian is diagonalized through a LAPACK subroutine and, with the eigenvalues and eigenvectors in hand, one should be able to compute the observables. When the observable requires some algebra to find the final expression, the procedure is shown in the appendices.

Some quantities of interest may take a considerable amount of time to give a reliable precision. Thus, to reduce this computation time one can diagonalize H^2 instead of H. With this trick the problem changes to diagonalizing two $L/2 \times L/2$ matrices instead of one $L \times L$ matrix. Taking the square of Eq. 2.20 and making the following change of basis $\{|1\rangle, |2\rangle, |3\rangle, \cdots, |L-1\rangle, |L\rangle\} \rightarrow \{|1\rangle, |3\rangle, |5\rangle, \cdots, |L-1\rangle, |2\rangle, |4\rangle, |6\rangle, \cdots, |L\rangle\}$, where $|i\rangle$ represents the i-th site, gives a block diagonal matrix. The upper left block H^2_{odd} corresponds to fermions hopping in the odd lattice, and it is given by

$$H^2_{odd} = \begin{pmatrix} J_1^2 + \left(aJ_{\frac{L}{2}}\right)^2 & aJ_1^2 & 0 & \cdots & (-1)^{N+1} aJ^2_{\frac{L}{2}} \\ aJ_1^2 & J_2^2 + (aJ_1)^2 & aJ_2^2 & \cdots & 0 \\ 0 & aJ_2^2 & \ddots & \ddots & \\ \vdots & \cdots & \ddots & J^2_{\frac{L}{2}-1} + \left(aJ_{\frac{L}{2}-2}\right)^2 & aJ^2_{\frac{L}{2}-1} \\ (-1)^{N+1} aJ^2_{\frac{L}{2}} & \cdots & & aJ^2_{\frac{L}{2}-1} & J^2_{\frac{L}{2}} + \left(aJ_{\frac{L}{2}-1}\right)^2 \end{pmatrix}, \tag{2.23}$$

while the matrix for fermions hopping in the even lattice is

$$H^2_{even} = \begin{pmatrix} J_1^2\,(1+a^2) & aJ_1J_2 & 0 & \cdots & (-1)^{N+1}\,aJ_{\frac{L}{2}}J_1 \\ aJ_1J_2 & J_2^2\,(1+a^2) & aJ_2J_3 & \cdots & 0 \\ 0 & aJ_2J_3 & \ddots & \ddots & \\ \vdots & \cdots & \ddots & J^2_{\frac{L}{2}-1}\,(1+a^2) & aJ_{\frac{L}{2}-1}J_{\frac{L}{2}} \\ (-1)^{N+1}\,aJ_{\frac{L}{2}}J_1 & \cdots & & aJ_{\frac{L}{2}-1}J_{\frac{L}{2}} & J^2_{\frac{L}{2}}\,(1+a^2) \end{pmatrix}. \tag{2.24}$$

The $(L/2+i)$-th eigenvalue of H is equal to the square root of the i-th eigenvalue of either H^2_{odd} or H^2_{even}. The eigenvectors of the original Hamiltonian can also be retrieved, as it is shown in Appendix A.

However, despite the reduction of computation time, one should be considerate while calculating observables from the eigenvalues or eigenvectors of the squared Hamiltonian. As it is discussed in Appendix B, the precision of this method is only reliable for $D \leq 2.0$.

3 Critical exponents of the XX model with correlated disorder

This chapter gives the full set of critical exponents, namely $\{\alpha, \beta, \gamma, \delta, \eta, \nu\}$, of the XX_{CD} model. The chapter is divided in two sections, one for the system at the critical point ($a = 1$) and the other for the system out of criticality ($a \neq 1$). In each section the quantities of interest are calculated for various disorder strengths D. The corresponding critical exponents are determined via linear regression and are usually shown as a function of D. Furthermore, the four scaling relations between the exponents are investigated and it is shown that two of them are only satisfied for the clean system ($D = 0$), while the other two still hold for $D > 0$.

3.1 Exponents at criticality

At criticality there is the correlation function exponent η to be determined; the other critical exponents are found exclusively out of criticality. Besides η, here are also determined the so-called critical dynamical exponent z and two thermodynamic exponents α_T and γ_T which are related to the specific heat and the magnetic susceptibility, respectively. The thermodynamic quantities are shown in the first part of this section, whereas the second one is dedicated to correlation function calculations.

It is important to remark, though, that in general the observables for a disordered system are averages and, therefore, have an associated error. Here, however, the error bars are not shown for simplicity, mostly because they are about the size of the points. Moreover, the errors of the critical exponents given by the fitting method are also neglected, since they may not represent the actual uncertainty. Instead, it is considered an a priori absolute error in the order of 10^{-2} for every critical exponent, which is the usual precision in studies of critical behavior.

3.1.1 Dynamical and thermodynamic exponents

The first exponent evaluated here is the critical dynamical exponent z. This exponent establishes an interplay between the relaxation time ξ_τ and the correlation length ξ by the relation $\xi_\tau \sim \xi^z$. To determine z without considering the temporal evolution of the system, one can replace the typical time scale ξ_τ with the inverse of the typical energy scale, i.e. $\xi_\tau \sim \Delta^{-1}$, where Δ is the gap energy. Moreover, the finiteness of the system prevents the divergence of the correlation length at criticality. Thus, according to finite-size scaling methods (37, 38), one can replace ξ by the lattice size L, which yields

$$\Delta \sim L^{-z}. \tag{3.1}$$

The gap Δ in the equation above is defined as the energy difference between the first excited state $|\psi_1\rangle$ and the ground state $|GS\rangle$. The first excited state is built by creating the lowest-energy particle above the Fermi level, i.e.

$$|\psi_1\rangle = \eta^\dagger_{\frac{L}{2}+1} |GS\rangle \,. \tag{3.2}$$

Notice that the additional fermion changes the sign of the boundary term in the Hamiltonian. Thus, for each disorder realization one must diagonalize two matrices, one for $N = L/2$ and another for $N = L/2 + 1$. Denoting the i-th eigenvalue of the former and the latter matrices as λ_i and λ'_i, respectively, the gap energy is, thereby,

$$\Delta \;=\; \sum_{i=1}^{\frac{L}{2}-1} \lambda'_i - \sum_{i=1}^{\frac{L}{2}} \lambda_i. \tag{3.3}$$

Fig. 3 shows the plot of Δ vs. L for various disorder strengths D. The correlated disorder case is also compared to the uncorrelated one. Notice that the curves of the former respect the power-law scaling and have a disorder varying slope, while the curves of the latter start to bend as L increases. The bending is a signature of the activated scaling, which is a known feature of the IRCP. For $D = 0.1$ this behavior cannot be observed because L is much smaller than the so-called crossover length ξ_C; only for $L \gg \xi_C$ the true scaling behavior of the system is achieved.

From Fig. 3 it is clear that exists a disorder-dependent crossover length for the uncorrelated chain. Indeed, previous studies show this crossover for other quantities of interest. (39, 40) Conversely, it turns out that for the XX_{CD} model there is no such crossover length, as indicated by renormalization group studies. (41) The proof of this statement, however, is beyond the scope of the present work.

The curves slope in Fig. 3 correspond to the critical dynamical exponent, which is shown as a function of disorder strength in Fig. 4*. From this figure one can notice that

*The plot of z vs. D has already been reported (9), but here a wider disorder range was considered.

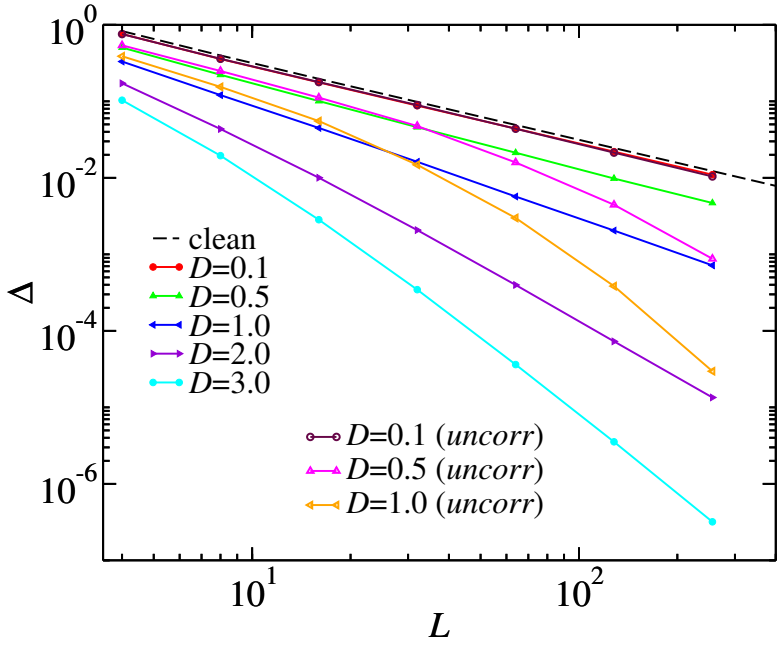

Figure 3 – Gap energy Δ vs. the chain size L for several disorder strengths D. For $D \leq 1.0$ it is also shown the gap for the uncorrelated (uncorr) case. The data points were averaged until its relative error was about 1%. The black dashed line corresponds to the clean system. The colored lines are guide to the eyes.

Source: By the author.

the CCP is preserved up to a critical disorder $D_C \approx 0.3$. For stronger disorder ($D > D_C$) the system falls into a line of FDCPs, where the critical dynamical exponent z grows linearly with D. Moreover, one can compare the two sets of data points and observe that they approach the line $z = D + 1/2$ as the exponent is fitted from larger chains. This line, however, was not predicted theoretically; it is rather an observation.

Besides the critical dynamical exponent, one can also evaluate the exponents of the specific heat C and the magnetic susceptibility χ. These quantities are defined as derivatives of the free energy. Thus, one must consider finite temperature to use statistical mechanics methods and compute the partition function and, consequently, the free energy (for more details see Appendix C). After some algebra one can find the following expressions

$$C = \frac{1}{2T^2 L} \sum_{i=1}^{\frac{L}{2}} \lambda_i^2 \cosh^{-2}\left(\frac{\lambda_i}{2T}\right), \tag{3.4}$$

$$\chi = -\frac{1}{2TL} \sum_{i=1}^{\frac{L}{2}} \cosh^{-2}\left(\frac{\lambda_i}{2T}\right). \tag{3.5}$$

It is expected that the thermodynamic quantities above exhibit a power-law behavior with respect to the temperature T, i.e. $C \sim T^{\alpha_T}$ and $\chi \sim T^{\gamma_T}$ at criticality. Fig. 5 shows a plot of the specific heat vs. the temperature for the clean system and various lattice sizes. Notice that there is a region where the power-law scaling is violated. This region corresponds to temperature values that are smaller than the finite-size gap. Thus, since the

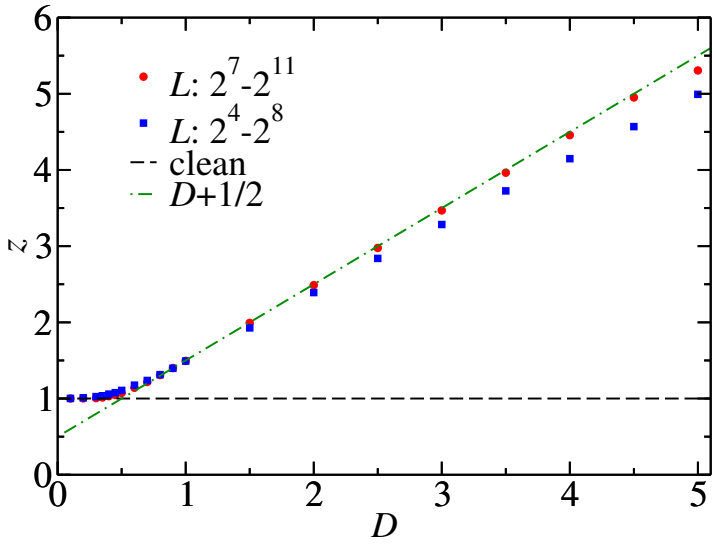

Figure 4 – Critical dynamical exponent z vs. disorder strength D. The exponent was fitted from the finite-size gap, as in Fig. 3, for two ranges of L varying as a power of two. The black dashed line represents the clean exponent value.

Source: By the author.

gap is inversely proportional to L, the range of temperature where the power-law scaling is observed is wider for larger chains, as one can verify in Fig. 5. Furthermore, T should not get large enough to the point where the thermal fluctuations overcome the quantum ones and the quantum critical behavior is lost. Therefore, one must assure that the fitting region fulfills $\Delta < T < 1$.

Setting $L = 2^{12}$ and $T = e^{-x}$, with x integer and $x \in [2, 6]$, the specific heat and the magnetic susceptibility were computed for various disorder strengths, averaging over 10^4 disorder realizations. The respective exponents α_T and γ_T were fitted from the data. Fig. 6 shows those exponents plotted as a function of disorder strength D. Notice that α_T and γ_T are related with the critical dynamical exponent z according to the following expressions

$$z = \frac{1}{\alpha_T}, \tag{3.6}$$

and

$$z = \frac{1}{\gamma_T + 1}. \tag{3.7}$$

This is in agreement with the results of the renormalization group methods introduced in Ref. (41).

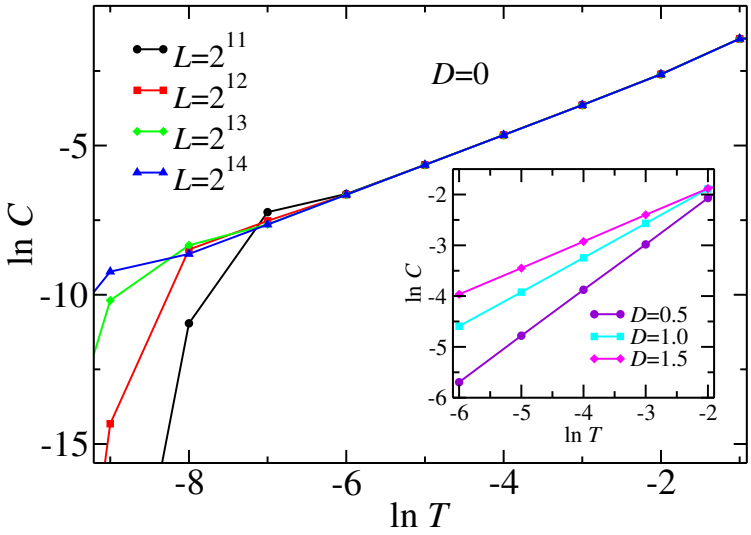

Figure 5 – Specific heat C vs. the temperature T for the clean chain ($D = 0$) at criticality for various chain sizes L. Inset: C vs. T for various disorder strengths D and lattice size $L = 2^{12}$, averaged over 10^4 disorder realizations. The lines are guide to the eyes.

Source: By the author.

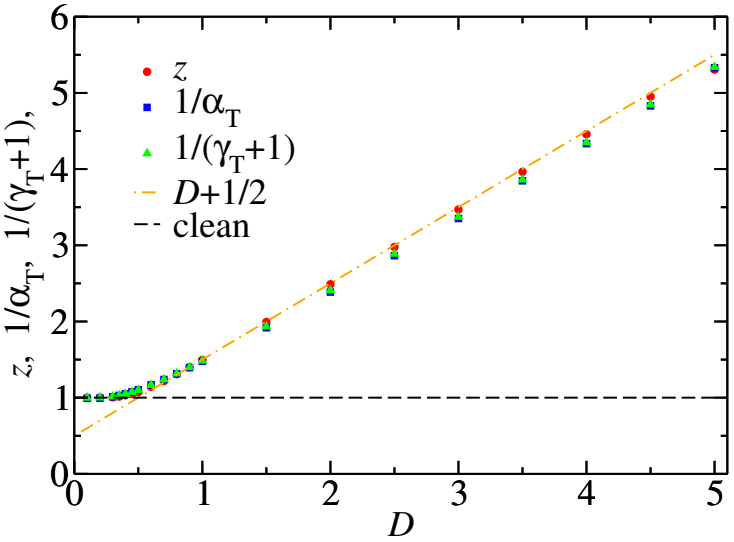

Figure 6 – Comparison between the critical dynamical exponent z (red circles) and the thermodynamic exponents at criticality α_T and γ_T of the specific heat C and the magnetic susceptibility χ, respectively. The exponents are plotted vs. the disorder strength D. The thermodynamic exponents were fitted for every value of D from the data similar to the inset of Fig. 5, using the same temperature range and chain size $L = 2^{12}$. The critical dynamical exponent is a reproduction of Fig. 4.

Source: By the author.

3.1.2 Spin-spin and dimer-dimer correlation functions

The spin-spin correlation function in the α-direction is defined as

$$G^{\alpha}(r) = \left\langle S_i^{\alpha} S_j^{\alpha} \right\rangle - \langle S_i^{\alpha} \rangle \left\langle S_j^{\alpha} \right\rangle, \tag{3.8}$$

where $r = |j - i|$ is the distance between spins. It was discussed in Chapter 2 that the single-operator average vanishes, i.e. $\langle S_i^{\alpha} \rangle = 0$, which leaves only the double-operator average $\left\langle S_i^{\alpha} S_j^{\alpha} \right\rangle$ to be determined. Appendix D outlines the procedure to compute $\left\langle S_i^{\alpha} S_j^{\alpha} \right\rangle$ for the longitudinal ($\alpha = z$) and transverse ($\alpha = x$) components. Here the y-component is equivalent to x one, since the system is invariant under a rotation of $\pi/2$ about the z-axis.

It is known that the correlation function scales as

$$\overline{G^{\alpha}(r)} \sim r^{-a_{\alpha}} \exp\left(-\frac{r}{\xi}\right), \tag{3.9}$$

where $\overline{\cdots}$ represents the average[†]. Thus, since the correlation length diverges at criticality, i.e. $\xi \to \infty$, $G^{\alpha}(r)$ should scale as a power law. Fig. 7 shows the x and z-components of the spin-spin correlation function for various disorder strengths D and chain size $L = 1024$. The data were averaged over 10^3 disorder realizations. Taking the absolute value is necessary to show the log-log plot, since $G^{\alpha}(r)$ has negative values. Notice that the power-law scaling is respected for the longitudinal and transverse components. The curves of the former, however, do not change significantly as disorder gets stronger, but for the latter the slope is clearly disorder dependent.

Fig. 7 also compares the average correlation to the typical one $G^{\alpha}_{typ}(r)$, which is defined as

$$G^{\alpha}_{typ}(r) = \exp\left[\overline{\ln G^{\alpha}(r)}\right]. \tag{3.10}$$

Comparing the average and typical correlations may provide a further understanding about the random critical point. For instance, it has been observed that for a system in an FDCP the average and typical correlations display similar behaviors, whereas for the IRCP those quantities behave differently from each other. (42) Indeed, for the uncorrelated disorder case it has been shown that $G^{\alpha}_{typ}(r)$ scales exponentially instead of the power-law scaling of the average correlation. (23) Thus, the purpose of computing the typical correlation of the XX_{CD} model is to contrast with the known results for the uncorrelated disorder case.

From the plot of Fig. 7, and within the region $1 \ll r \ll L$, one can also determine the critical exponent a_{α} for each of the correlation functions. Fig. 8 shows a_{α} vs. the disorder strength D for $\alpha = x$ and $\alpha = z$. Notice that the former is different than the latter, which is in agreement with the results for the clean chain. Conversely, for the uncorrelated

[†]For simplicity, hereafter the average symbol $\overline{\cdots}$ is dropped, but recall that for random systems all measurements are averages.

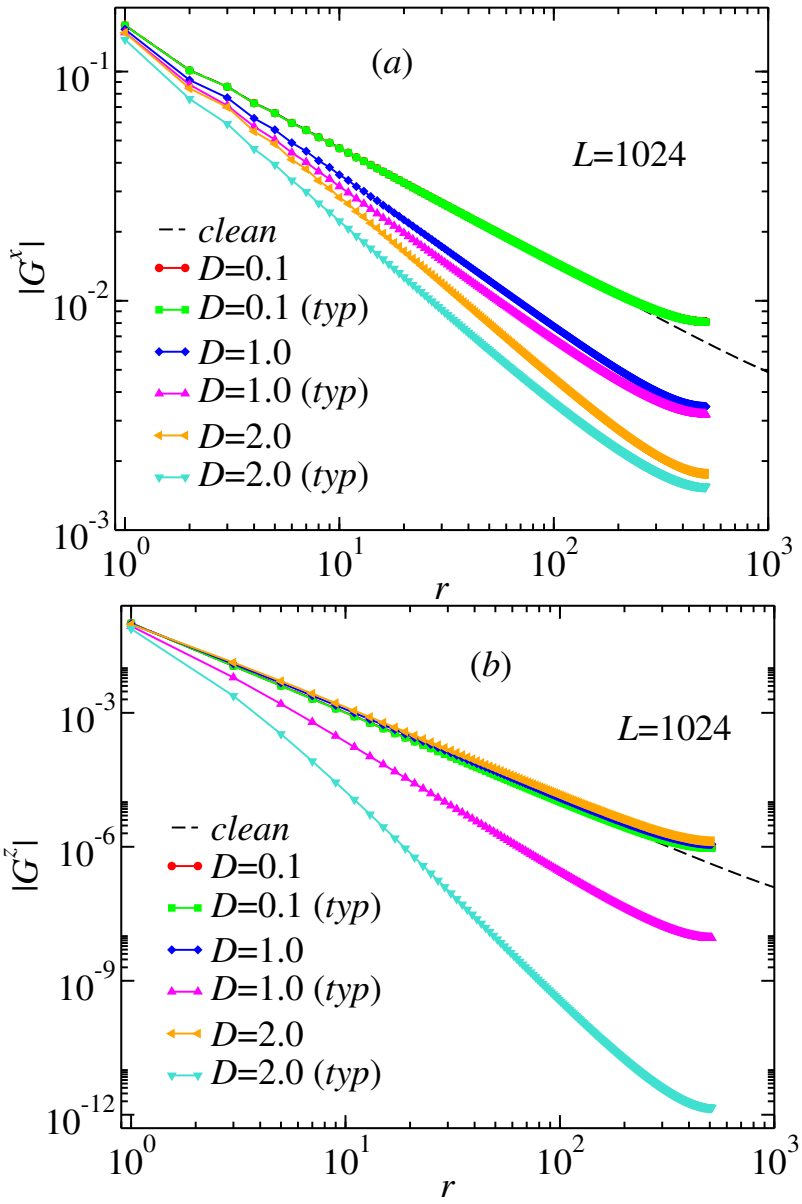

Figure 7 – Average and typical (typ) spin-spin correlation function for various disorder strengths D and lattice size $L = 2^{10}$. Panels (a) and (b) show the x and z-components, respectively. The data were averaged over 10^3 disorder realizations. Some curves are overlapped with the black dashed line, which corresponds to the clean chain with size $L = 2^{12}$.

Source: By the author.

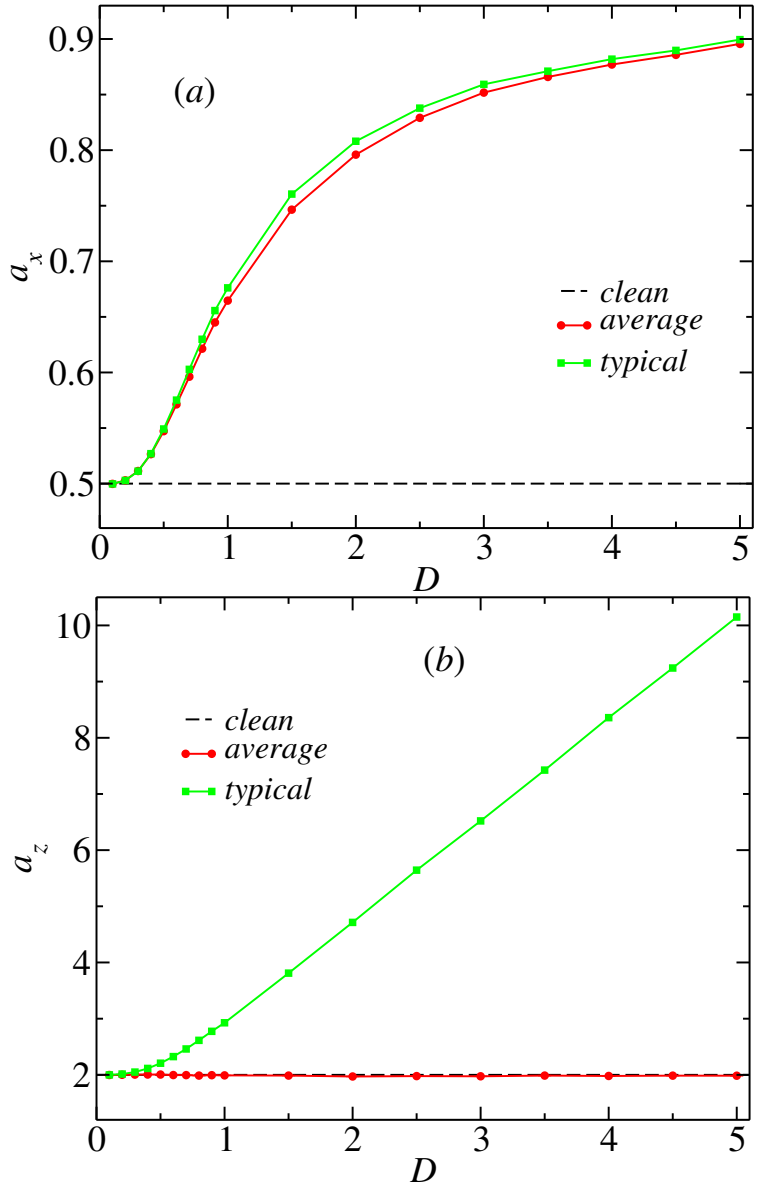

Figure 8 – Critical exponent a_α of the average and typical spin-spin correlation function vs. disorder strength D. Panels (a) and (b) correspond to $\alpha = x$ and $\alpha = z$, respectively. The exponents were fitted from the data of the correlation, as shown in Fig. 7, for chain size $L = 2^{10}$ and within the region $1 \ll r \ll L$. The black dashed line is the clean exponent value. The colored lines are guide to the eyes.

Source: By the author.

disorder case it has been shown that $a_x = a_z$, regardless of D. (40) Furthermore, for the transverse component, the exponent of the average correlation grows with D in a similar fashion as the exponent of the typical one. For the longitudinal component, though, $a_z = 2.0$ for every value of D, whereas the exponent of the typical correlation grows linearly with disorder for $D > D_C$.

Knowing the correlation function exponent a_α allows one to determine the critical exponent η. However, for the XX model in general (i.e. for the clean and random cases) one

should not evaluate η from the spin-spin correlation function. The actual exponent must come from the correlation function of the operator that gives the order parameter of the model. For instance, the sum of the spin operator S_i over the chain gives the magnetization. This quantity, though, is not a suitable order parameter for the XX model, since it is equal to zero in the ordered phase.

Therefore, one must define another operator that yields a valid order parameter for the XX model. Here it is chosen the so-called dimer operator M_i, which is defined as

$$M_i \equiv -\left(S^x_{2i-1}S^x_{2i} + S^y_{2i-1}S^y_{2i}\right) + \left(S^x_{2i}S^x_{2i+1} + S^y_{2i}S^y_{2i+1}\right). \tag{3.11}$$

The index i represents the i-th dimer of the chain. One can check for the clean chain that $\langle M_i \rangle = 0$ at criticality and $\langle M_i \rangle \neq 0$ in the ordered phase. The corresponding order parameter m of the dimer operator is defined as the average over the lattice of the dimer operator M_i, i.e.

$$m = \frac{2}{L}\sum_{i=1}^{\frac{L}{2}} \langle M_i \rangle . \tag{3.12}$$

It is important to remark, though, that the choice of the order parameter for a model may not be unique; the only requirement is that it must be zero at the critical point and nonzero out of criticality. For the XX model, for example, it has also been proposed the so-called string order parameter. (42–44)

With the definition of the dimer operator in Eq. 3.11, one can now compute the dimer-dimer correlation function $G^{dd}(r)$, which is given by

$$G^{dd}(r) = \langle M_i M_j \rangle - \langle M_i \rangle \langle M_j \rangle . \tag{3.13}$$

Fig. 9 shows the typical and average $G^{dd}(r)$ for various disorder strengths D and lattice size $L = 1024$. The samples were averaged over 10^4 disorder realizations. Notice that for weak disorder ($D < D_C$) the typical correlation coincides with the average one. As disorder increases, though, the slope of the former varies more rapidly. This can be verified in Fig. 10, which gives the plot of the exponents a_{dd} as a function of D for the average and typical correlations.

3.2 Exponents at the dimer phase (out of criticality)

Similarly to the previous section, this one is divided in two parts. The first part is dedicated to the thermodynamic quantities, while the second one provides the study of the correlation function. In the first part the thermodynamic critical exponents, namely

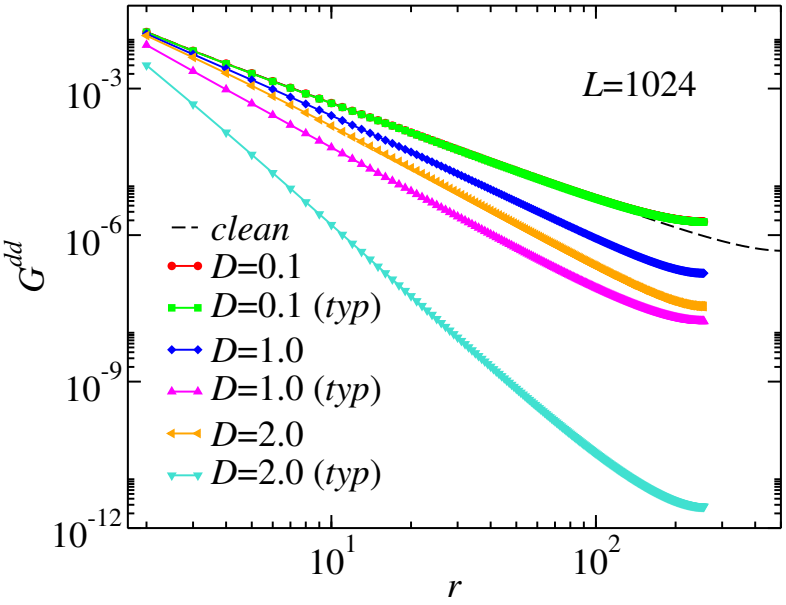

Figure 9 – Average and typical (typ) dimer-dimer correlation function for various disorder strengths D and chain size $L = 2^{10}$. The data were averaged over 10^4 disorder realizations. The black dashed line corresponds to the clean chain with size $L = 2^{12}$.

Source: By the author.

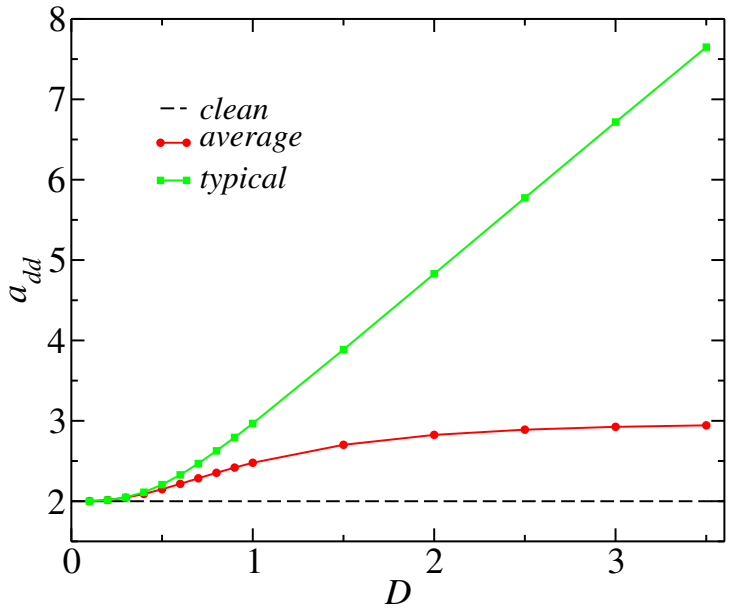

Figure 10 – Critical exponent a_{dd} of the average and typical dimer-dimer correlation function vs. disorder strength D. The exponents were fitted from the data of the correlation, as shown in Fig. 9, for lattice size $L = 2^{10}$ and within the region $1 \ll r \ll L$. The black dashed line is the clean exponent value. The colored lines are guide to the eyes.

Source: By the author.

$\{\alpha, \beta, \gamma, \delta\}$, are determined and the respective scaling relations are tested. The last critical exponent ν is determined in the second part, where the other two scaling relations are also investigated.

3.2.1 Thermodynamic exponents

Before discussing the quantities that give the remaining critical exponents, it is investigated here what happens to the gap energy Δ when the system is driven out of criticality. It has been already reported that for clean half-integer spin chains the gap is closed ($\Delta = 0$) at criticality and it begins to open as the system is driven out of the critical point. (45,46) The numerical results from the previous section show that the finite-size gap of the clean and correlated-random chains exhibit a power-law decay with the chain size L, i.e. $\Delta \sim L^{-z}$. Thus, at the thermodynamic limit ($L \to \infty$) both systems are gapless. However, it is shown in the following that in the ordered (dimer) phase the XX_{CD} model behaves differently from the clean chain; the gap is still closed out of criticality.

Fig. 11 shows the gap Δ plotted as a function of θ for various lattice sizes and two values of disorder strength. Plotting an observable for various L allows one to determine whether the displayed behavior represents the one expected at the thermodynamic limit. For instance, if the separation between curves for a fixed D diminishes as L increases one may conclude that the observed behavior is correct. This is clearly not the case for $D = 1.0$, where the separation between curves remains approximately constant. Thus, the gap in Fig. 11 for $D = 1.0$ is due to finite-size effects; for a sufficiently large chain the system is gapless. However, for $D = 0.1$ one cannot derive the same conclusion by analyzing Fig. 11 alone.

The reason why the gap is indeed closed even for every value of D is that the introduction of randomness provides a nonzero probability of existing a region of size l where the couplings are small. The probability of finding such region increases with lattice size L and disorder strength D. Furthermore, this region of small couplings will dominate the behavior of the system only if it is much larger than the characteristic scale of the system, i.e. $l \gg \xi$. One can test this statement with the following model: the clean chain is divided in two complementary parts, A and B of sizes l and $L - l$, respectively. For the subsystem A the constant coupling is defined as $J_A = 0.1$, while for the subsystem B the coupling is $J_B = 1$. The gap energy Δ is thus calculated for various l.

Fig. 12 shows Δ vs. l for three distances from criticality. Notice that, as expected, there is a transient behavior where the ratio Δ/θ approaches J_B as $\xi \gg l$ and J_A as $l \gg \xi$. The inset of Fig. 12 shows the average minimum coupling J_{min}, evaluated from 10^5

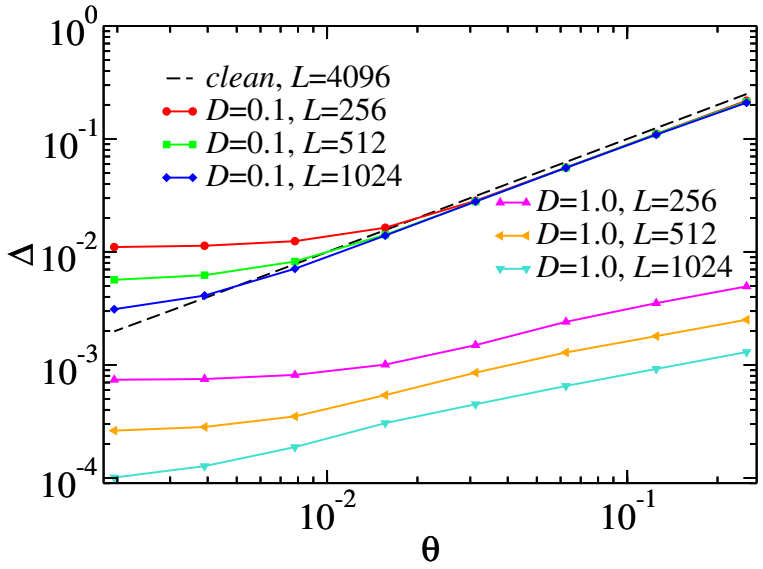

Figure 11 – Gap energy Δ vs. distance from criticality θ for disorder strength $D = 0.1$ and $D = 1.0$ and chain sizes L. The samples were averaged until the relative error was about 1%. The black dashed line corresponds to the clean chain with $L = 4096$. The colored lines are guide to the eyes.

Source: By the author.

disorder realizations, vs. the chain size L for three disorder strengths. Observe that J_{min} decays with an exponent equal to D. Thus, neglecting the disorder dependent prefactor, to get a J_{min} for $D = 0.1$ close to the one obtained for $D = 1.0$ one should consider a lattice L^{10} times larger. Therefore, one can conclude that the XX_{CD} model is also gapless in the ordered phase regardless of disorder strength; the gap in Fig. 11 is due to finite-size effects. This conclusion can be extended for every random spin-1/2 chain with a probability distribution that allows couplings close enough to zero.

After discussing what happens to the gap energy out of criticality, the focus returns to determining the critical exponents. The first one evaluated here is α, which is related to the specific heat. Differently from the previous section, the exponent is now determined by varying θ and setting $T = 0$. However, the problem is how one can compute specific heat without temperature, since this quantity is defined as the derivative of the internal energy with respect to T.

Using the statistical mechanics definition of C, one can make an analogy and define a specific heat C' for QPTs. For instance, at $T = 0$ the ensemble-averaged (internal) energy corresponds to the ground-state energy E_0. Furthermore, for the XX model the constant a is the parameter that has the same role of temperature for classical transitions. Thus, C' can be defined as

$$C' = \frac{\partial E_0}{\partial \theta}, \tag{3.14}$$

where it was used that $d\theta = da$. Since the derivative in Eq. 3.14 cannot be calculated analytically, one must consider methods of numerical differentiation.

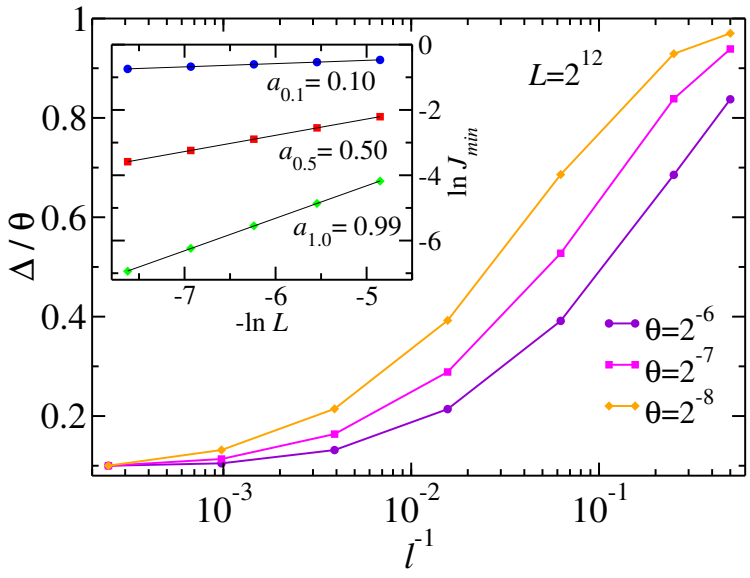

Figure 12 – Gap energy Δ of the clean chain divided in two subsystem A and B of sizes l and $L-l$, respectively. The former has couplings $J_A = 0.1$, whereas the latter has couplings $J_B = 1.0$. The gap energy Δ is plotted as a function of l for various distances from criticality θ. The lines are guide to the eyes. Inset: Average minimum coupling J_{min} vs. the chain size L for three disorder strengths D, averaged over 10^5 disorder realizations. The black lines are the best fit with respective exponent a_D.

Source: By the author.

Fig. 13 shows the plot of C' as a function of θ for various disorder strengths D. The ground-state energy E_0 was computed for $\theta = 2^{-x}$, with x integer and $x \in [2, 9]$, and averaged over 10^5 disorder realizations. The plot of E_0 vs. θ was interpolated using a cubic spline, giving 12 equally spaced points. The data from Fig. 13 correspond to the centered differentiation of the interpolated lines. Notice that C' becomes smaller as disorder is increased.

Moreover, it is possible to affirm from Fig. 13 that all curves are consistent with an exponent $\alpha = 0$, even though the rule of thumb for determining critical exponents was not respected. This rule states that one should consider at least three orders of magnitude for θ to obtain a reliable estimate for the exponent. One can notice, however, that the curves tend to a constant as they approach criticality. Thus, to consider smaller θ the number of disorder realizations should increase to guarantee that a given point does not have a greater E_0 than another one to its right side. If, however, the ground-state energy is calculated with a poor statistics, the numerical differentiation may provide misleading results.

The next critical exponent evaluated is γ, which describes the scaling of the susceptibility χ with respect to θ. The susceptibility can be calculated from the dimer-dimer correlation function $G^{dd}(r)$. According to the fluctuation-dissipation theorem (18),

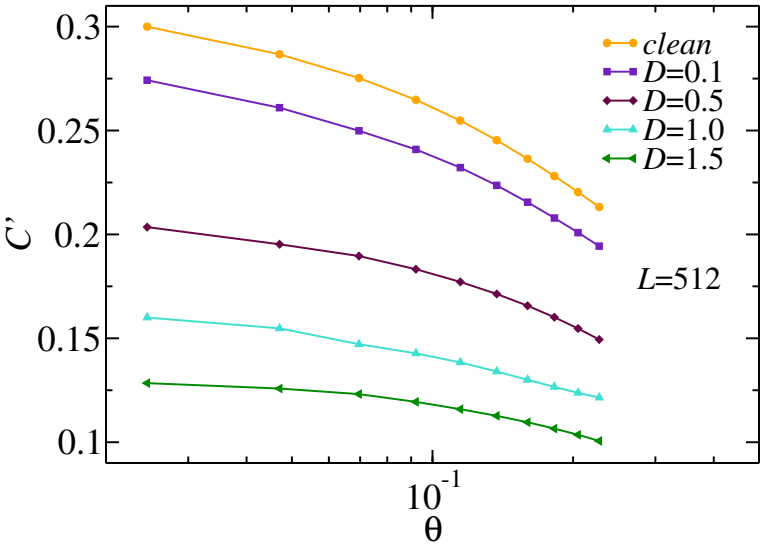

Figure 13 – Specific heat C' of the quantum phase transition vs. the distance from criticality θ for several disorder strength D and lattice size $L = 512$. The data were obtained from the differentiation of the ground-state energy E_0 with respect to θ. Each E_0 was averaged over 10^5 disorder realizations. The lines are guide to the eyes.

Source: By the author.

the susceptibility is proportional to the sum of the $G^{dd}(r)$ over the distance r, i.e.

$$\chi \propto \sum_{r=1}^{\frac{L}{4}} G^{dd}(r)\,. \tag{3.15}$$

Fig. 14 shows the susceptibility χ vs. the distance from criticality θ for several disorder strengths D. The susceptibility was calculated from $G^{dd}(r)$ averaged over 10^3 disorder realizations and for chain size $L = 512$. Notice that χ behaves similar to C'; it tends to a constant as θ gets closer to zero. Thus, one can conclude once again that the data are consistent with a critical exponent $\gamma = 0$.

The last thermodynamic quantity to be evaluated is the order parameter m, as defined in Eq. 3.12. It is important to remark that the dimer operator calculated out of criticality exhibits an unexpected behavior. Fig. 15 shows the dimer operator M_i vs. its respective position i for various disorder strengths D and chain size $L = 128$. Notice that there are some points where $M_i < 0$; i.e. they are at even dimer phase. This was not expected to occur for the XX_{CD} model, since the correlation between couplings followed by the dimerization should assure that the odd sublattice had stronger couplings than the even one. Thus, M_i should be positive all over the chain. Indeed, one can verify this for the clean chain.

The introduction of randomness in the chain apparently creates a collective effect that allows the existence of negative values of M_i. Nonetheless, one can observe in Fig. 15 that the density of points above the dashed line is greater than below. If, however, the

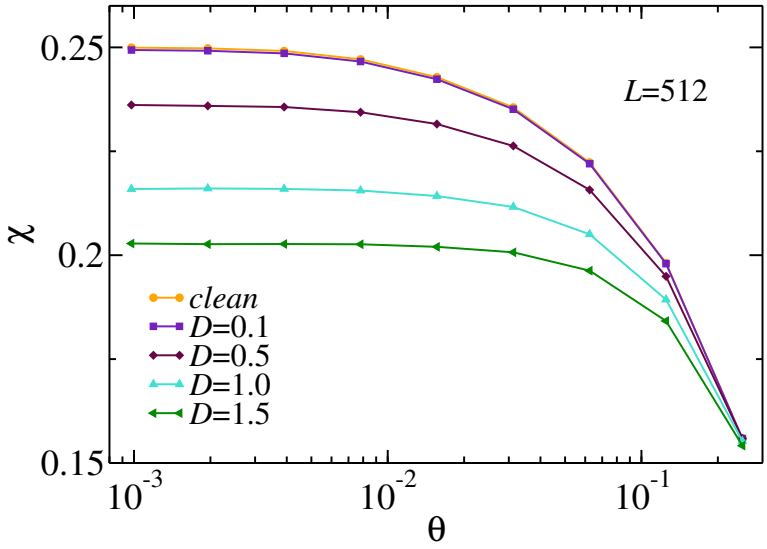

Figure 14 – Susceptibility χ vs. the distance from criticality θ for several disorder strengths D. Here the susceptibility is the sum of the dimer-dimer correlation function $G^{dd}(r)$ over the distance r. $G^{dd}(r)$ was computed for chain size $L = 512$ and averaged over 10^3 disorder realizations. The lines are guide to eyes.

Source: By the author.

number of positive and negative points were equal to each other, the order parameter m would be zero and the system would be at the critical point.

For systems under random-T_C disorder, such as the uncorrelated random XX model, there is a nonzero probability of finding a relatively large region that is in a different phase than the bulk system. (47–49) These are known as rare regions and they usually dominate the behavior of the phase transition. (12, 50) However, even though Fig. 15 shows dimers at opposite phases, these rare regions are fundamentally different and do not play an important role at the QPT.

From the order parameter defined in Eq. 3.12 one can determine two critical exponents, viz. β and δ. To find the former the procedure is the same as before; i.e. plotting m vs. θ. Conversely, to find the other exponent the distance from criticality is fixed at $\theta = 0$ and the order parameter is plotted as a function of the so-called conjugate field B. The introduction of this field leads to a new Hamiltonian H', which is given by

$$\begin{aligned} H' &= H - B\sum_{i=1}^{\frac{L}{2}} M_i, \\ &= \sum_{i=1}^{\frac{L}{2}} (J_i + B)\left(S^x_{2i-1}S^x_{2i} + S^y_{2i-1}S^y_{2i}\right) + (J_i - B)\left(S^x_{2i}S^x_{2i+1} + S^y_{2i}S^y_{2i+1}\right), \end{aligned} \quad (3.16)$$

where $B > 0$. Thus, one just need to replace the odd and even couplings by $(J_i + B)$ and $(J_i - B)$, respectively.

Fig. 16 shows the order parameter m vs. the distance from criticality θ and the

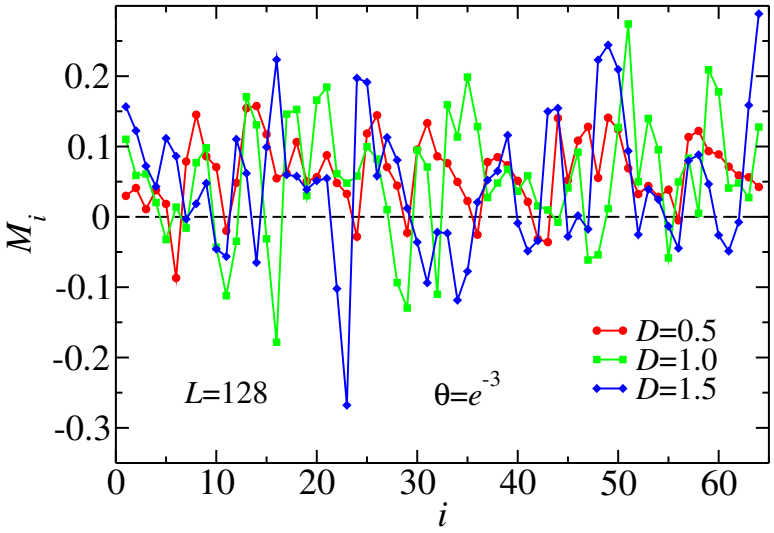

Figure 15 – Dimer operator M_i vs. the position i for various disorder strenghts D. It was considered a single disorder realization, with chain size $L = 128$ and distance from criticality $\theta = e^{-3}$. The lines are guide to the eyes.

Source: By the author.

Table 1 – The critical exponents β and δ fitted from Fig. 16 for several disorder strengths D.

Exponent	$D = 0.1$	$D = 0.5$	$D = 1.0$	$D = 1.5$
β	0.99	0.99	1.00	1.00
δ	1.00	1.00	1.01	1.09

Source: By the author.

conjugate field for various disorder strengths and lattice size $L = 512$. The data were averaged over 10^5 disorder realizations. The curves are compared to a dashed line with slope equal to clean exponent values, i.e. $\beta = 1.0$ and $1/\delta = 1.0$. Notice that the curves tend to become parallel to the dashed line as θ decreases. Table 1 gives the fitted exponent values for each disorder strength. The fitting region corresponds to the four leftmost points. Observe that only for $D = 1.5$ the δ exponent is relatively apart from the clean value; the others are in good agreement. Thus, to find a slope closer to unity one should consider smaller values of B.

From the results shown in this section, one can reasonably assume that for the XX_{CD} model the four thermodynamic critical exponents remain equal to the clean value as disorder is introduced. Furthermore, one can substitute $\alpha = \gamma = 0$ and $\beta = \delta = 1.0$ in the following scaling relations

$$2 - \alpha = 2\beta + \gamma, \tag{3.17}$$

$$2 - \alpha = \beta\,(\delta + 1)\,, \tag{3.18}$$

and check that they are indeed respected. However, one cannot assert from numerical results alone that the critical exponents are indeed disorder independent; other theoretical

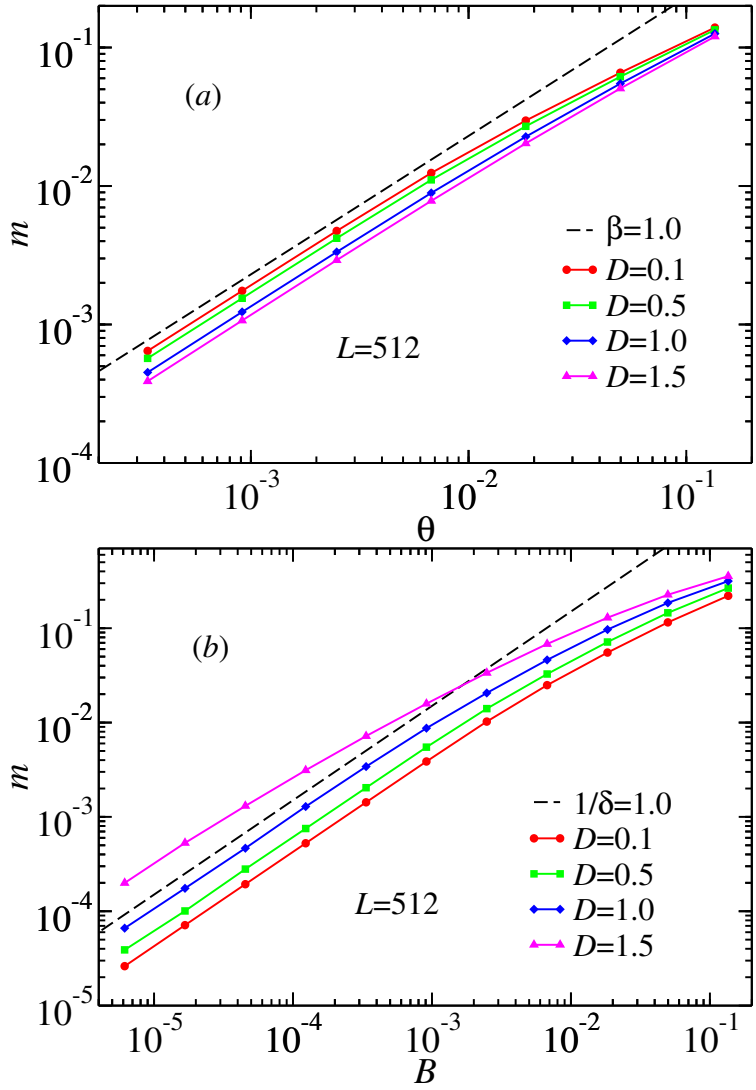

Figure 16 – Dimer order parameter m vs. (a) the distance from criticality θ and (b) the conjugate field B for several disorder strengths D and chain size $L = 512$. The data were averaged over 10^5 disorder realizations. Colored lines are guide to the eyes.

Source: By the author.

methods are required to prove the independence with respect to D. Nevertheless, it is rather unreasonable to believe that there may exists a disorder value above $D = 1.5$ from which the behavior of the system suddenly changes.

3.2.2 Spin-spin and dimer-dimer correlation functions

The last critical exponent to be determined is ν which describes the scaling of the correlation length ξ, i.e. $\xi \sim \theta^{-\nu}$. Thus, according to Eq. 3.9, one can find the correlation length from the linear regression of the logarithmic of the correlation function. Fig. 17

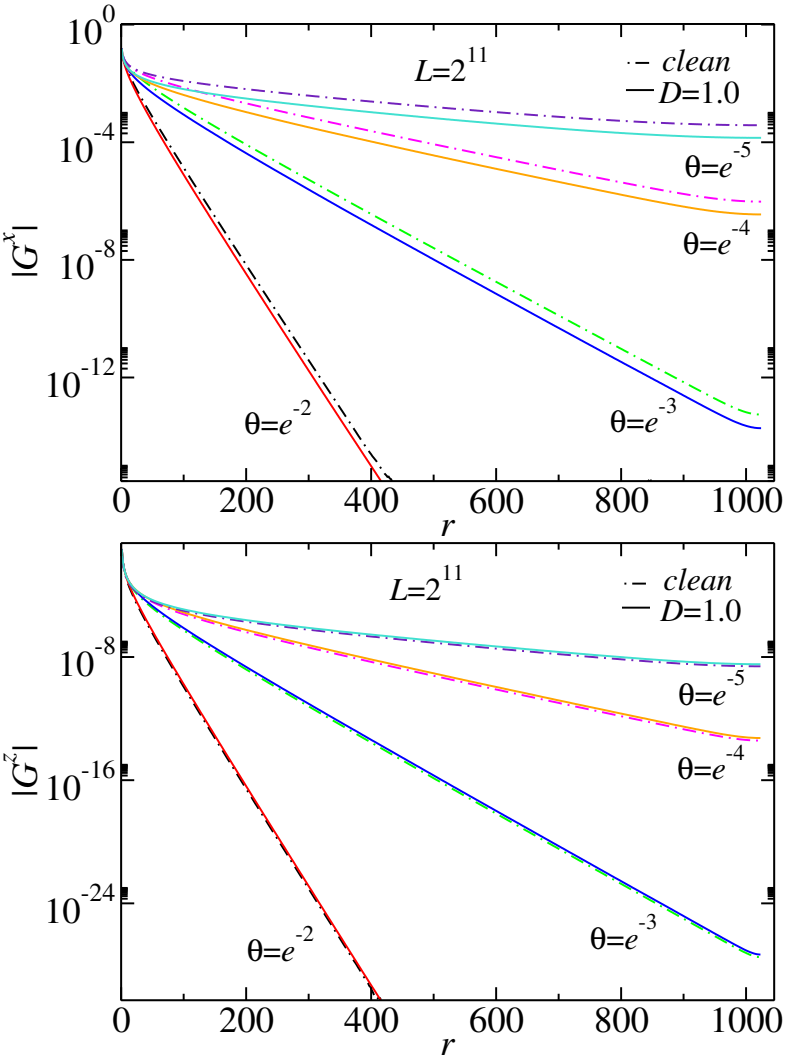

Figure 17 – The x and z-components of the spin-spin correlation function for various distances from criticality θ and lattice size $L = 2^{11}$. The dot-dashed lines correspond to the clean chain, while the continuous ones correspond to $D = 1.0$. The data were averaged over 10 and 10^3 disorder realizations for the x and z-directions, respectively.

Source: By the author.

and Fig. 18 show, respectively, the spin-spin and dimer-dimer correlation functions for several distances from criticality θ. Notice that for all correlation functions the behavior of the disordered chain with $D = 1.0$ (continuous lines) is similar to clean one (dot-dashed lines), which suggests that the correlation length exponent ν is disorder independent.

One can determine the critical exponent from the plot of ξ vs. θ. The correlation length can be fitted from Fig. 17 and Fig. 18 in the region where the curves are linear. However, notice that for $\theta = e^{-5}$ this linear behavior is not clear. This occurs when the correlation length is much larger than the lattice size (i.e. $\xi \gg L$) and the system is essentially at criticality and the power-law behavior dominates. Therefore, for the considered chain size ($L = 2^{11}$) there are only three points available to fit the exponent ν, which gives only one order of magnitude (e^{-2}–e^{-4}) in the range of θ. Nonetheless, one

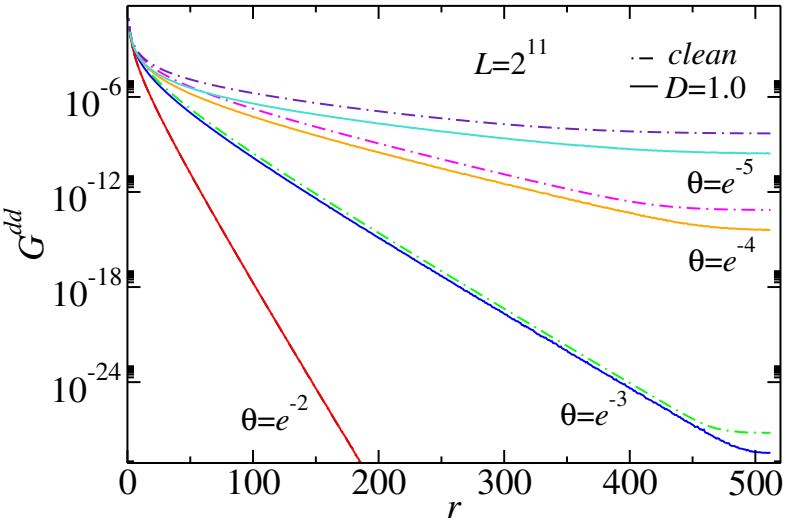

Figure 18 – Dimer-dimer correlation function $G^{dd}(r)$ for various distances from criticality θ and chain size $L = 2^{11}$. The dot-dashed lines correspond to the clean chain, while the continuous ones correspond to $D = 1.0$. The data were averaged over 10^4 disorder realizations.

Source: By the author.

Table 2 – Critical exponent ν_α and the correlation function exponent at criticality a_α for various disorder strengths D.

	x spin-spin: ν_x, a_x	z spin-spin: ν_z, a_z	dimer-dimer: ν_{dd}, a_{dd}
clean($D = 0$)	1.00(2), 0.50	1.00(2), 2.00	0.96(4), 2.00
$D = 0.5$	0.99(2), 0.55	1.00(2), 2.01	0.96(4), 2.15
$D = 1.0$	0.99(2), 0.66	1.00(2), 1.99	0.95(4), 2.48
$D = 1.5$	0.99(3), 0.75	1.00(2), 1.99	0.97(3), 2.70

Source: By the author.

can get a rough estimate of the exponent from just three points. If more data are desired one should consider larger chains, which may increase significantly the computation time required and, consequently, become unpractical.

Table 2 shows the fitted exponent ν for the spin-spin and dimer-dimer correlation functions, for various disorder strengths D. Notice that ν is indeed disorder independent, within the given error, for every correlation function. Furthermore, even though it is not possible to know the exact exponent value, one can conclude that ν is close to unity for the dimer-dimer correlation function, regardless of disorder strength. For the spin-spin correlations, $\nu = 1$ corresponds to clean chain exponent value, which can be determined exactly.

To check whether $\nu = 1$ is a good estimate for the critical exponent one can observe if the data shown in Fig. 17 and Fig. 18 collapse into a single universal function. One can determine this function from the scaling hypothesis, which states that the correlation

function $G^{\alpha}(r)$ is homogeneous with respect to its parameters (18, 19), i.e.

$$\lambda G^{\alpha}(r,\theta) = G^{\alpha}\left(\lambda^{a} r, \lambda^{b}\theta\right), \tag{3.19}$$

where λ, a and b are constants to be determined.

The first step is to eliminate the dependency on θ, which is achieved by making $\lambda^{b}\theta = 1$, yielding thereby

$$\theta^{-\frac{1}{b}} G^{\alpha}(r,\theta) = G^{\alpha}\left(r\theta^{-\frac{a}{b}}, 1\right). \tag{3.20}$$

It is also desired that the universal scaling Φ depends only in the parameter $x = r/\xi$, such that $\Phi(x)$ comprises the two limiting cases, namely the power-law ($x \to 0$) and exponential ($x \to \infty$) behaviors. Thus, since $\xi \sim \theta^{-\nu}$ one can find that $a/b = -\nu$, which gives

$$G^{\alpha}(r,\theta) = \theta^{\frac{1}{b}} \Phi\left(r\theta^{\nu}\right). \tag{3.21}$$

Furthermore, using that $\Phi(x) \sim x^{-a_{\alpha}}$ and $G^{\alpha}(r,\theta) \sim r^{-a_{\alpha}}$ in the limit $x \to 0$, one can find that $1/b = a_{\alpha}\nu$. Therefore, the universal scaling function is

$$\Phi\left(r\theta^{\nu}\right) = \frac{G^{\alpha}(r,\theta)}{\theta^{\nu a_{\alpha}}}. \tag{3.22}$$

Fig. 19 and Fig. 20 show $\Phi(x)$ for the spin-spin and dimer-dimer correlations, respectively, for the clean and disordered chains with $D = 0.1$ and $D = 0.5$. The distance r was replaced with the so-called chord length r', which is defined as

$$r' = \frac{L}{\pi} \sin\left(\frac{\pi r}{L}\right). \tag{3.23}$$

The chord length is the natural finite-size length of the clean critical chain. Here it is assumed that this correction is also valid for the XX_{CD} model. Indeed, Chapter 4 shows that this correction is satisfactory for the disordered chain. The chord length is employed to minimize finite-size effects, such as the curve bending in its rightmost end (see, for example, Fig. 17 and Fig. 18). Furthermore, to guarantee that all curves end in the same point it is fixed $L\theta = 16$.

Notice from Fig. 19 and Fig. 20 that the collapse fails for $r'\theta < 1$, except for the longitudinal spin-spin correlation. The reason of this failure can be the neglected further corrections of the power-law scaling. For instance, to obtain a more accurate exponent one should consider

$$G^{\alpha}(r) \propto \frac{1}{r^{a_{\alpha}}}\left(1 + \frac{1}{r^{b_{\alpha}}}\right), \tag{3.24}$$

or even more corrections. This is generally true for every quantity that exhibits power-law scaling. Conversely, the z spin-spin correlation shows a good collapse because it is known that for the clean chain the scaling is exactly

$$G^{z}(r') = -\frac{1}{(\pi r')^{2}}, \tag{3.25}$$

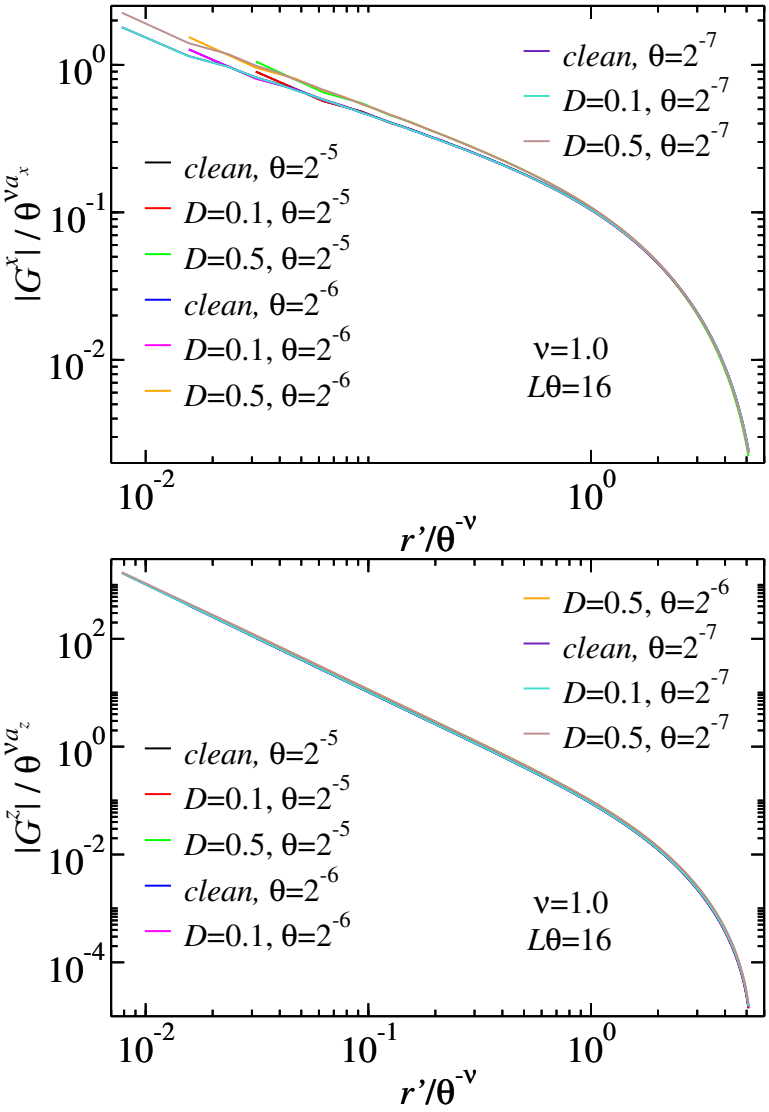

Figure 19 – Scaling of the x and z-component spin-spin correlation functions for various distances from criticality θ and disorder strengths D. The input exponent values a_x and a_z are shown in Table 2.

Source: By the author.

with r odd. Thus, since only relatively small D was considered in Fig. 19, the clean chain scaling is sufficient. If, however, one considers stronger disorder the curves would start to separate from each other, since disorder introduces further corrections that become more relevant as D increases.

Nevertheless, one should observe that the points below $r'\theta = 1$ correspond to about 6% of the chain. Thus, for the great majority of the lattice, the collapse is satisfactory for all the correlation functions evaluated. Therefore, the results suggest that for the XX_{CD} model the correlation length exponent ν is disorder independent and $\nu = 1$ is a reliable estimate.

Finally, with an estimate of the critical exponent ν one can now check the validity

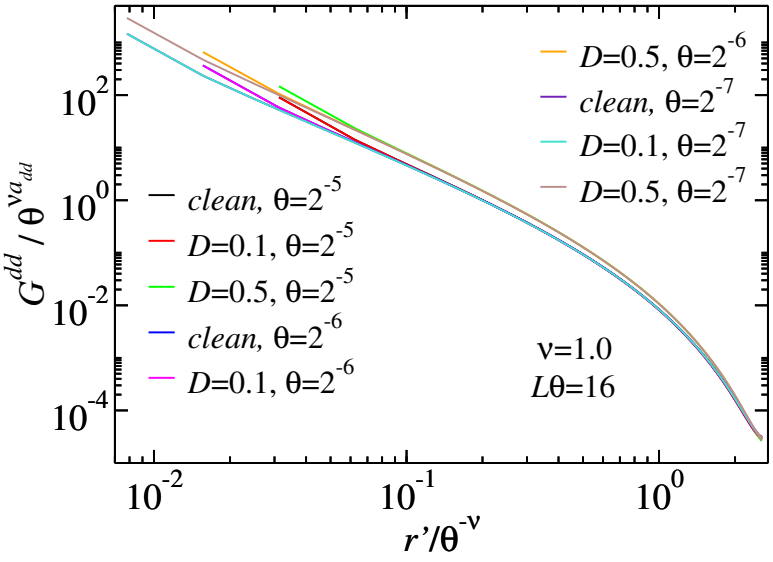

Figure 20 – Scaling of the dimer-dimer correlation function G^{dd} for various distances from criticality θ and disorder strengths D. The input exponent values a_{dd} are shown in Table 2.

Source: By the author.

of the other two scaling relations, viz.

$$\gamma = \nu\,(2 - \eta) \tag{3.26}$$

and

$$2 - \alpha = (d + z)\,\nu, \tag{3.27}$$

which are known as Fisher's scaling and hyperscaling relations, respectively. The original hyperscaling relation, though, does not include the critical dynamical exponent z. The substitution $d \to d + z$ is motivated from the quantum-to-classical mapping, which states that for a d-dimensional quantum critical system there is a classical $(d + z)$-dimensional equivalent. However, one should be concerned about this substitution, since not every quantum critical system have a classical counterpart. Nevertheless, if the critical dynamical exponent is not included the hyperscaling relation does not hold even for the clean chain.

Although replacing d with $d+z$ is necessary to fulfill the scaling relations, the Harris criterion in Eq. 2.17 does not require such replacement and the reason is the following: The quantum-to-classical mapping introduces an imaginary time direction where the couplings are constant instead of random. This extra direction, therefore, do not contribute to the distribution of distances from criticality, which was the starting point in the deduction of the criterion.

Even though it is not explicit, Eq. 3.26 also depends on the critical dynamical exponent z, because of the relation between η and a_{dd} which is given by

$$\eta = a_{dd} - (d + z) + 2. \tag{3.28}$$

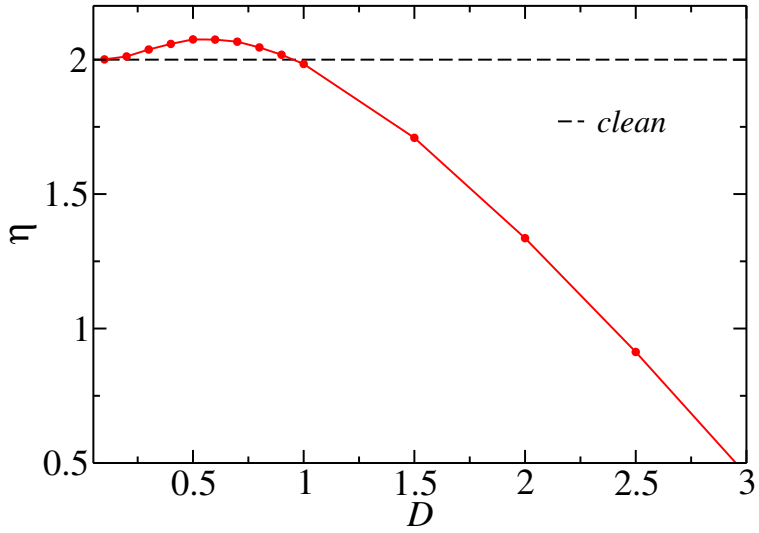

Figure 21 – Critical exponent η vs. the disorder strength D. The dashed line gives the clean chain exponent value. The red line is a guide to the eye.

Source: By the author.

Fig. 21 shows the anomalous dimension η vs. the disorder strength D. This exponent was obtained by inserting in Eq. 3.28 the values of a_1 and z from Fig. 10 and Fig. 4, respectively. Fisher's scaling relation would hold for every disorder strength if $\eta = 2$, since $\gamma = 0$ and $\nu = 1$. However, according to Fig. 21, Eq. 3.26 fails for the XX_{CD} model with disorder strength $D > D_C$. One could say that the scaling relation is respected up to $D = 1.0$ if there were points distributed above and below the dashed line in the region $D_C \leq D \leq 1.0$; one cannot trust, though, the curve pattern shown in Fig. 21.

Moreover, it is clear that the hyperscaling relation in Eq. 3.27 also fails for $D > D_C$. The breakdown of the hyperscaling relation is a known characteristic of systems that are above the so-called upper critical dimension d_c^+. For instance, the mean-field Ising model (which is above d_c^+) has exponents $\alpha = 0$ and $\nu = 1/2$, thereby violating Eq. 3.27.

Recently, though, it has been proposed that the hyperscaling relation for systems with $d \geq d_c^+$ should be rewritten as (51)

$$2 - \alpha = \frac{\nu d}{q}, \tag{3.29}$$

where $q = d/d_c^+$. Notice that for Eq. 3.29 the substitution $d \to d + z$ is not important, since d cancels out. However, for the XX model the upper critical dimension is $d_c^+ = 3$ and, consequently, Eq. 3.29 does not hold. Similarly, it has also been suggested a different Fisher's scaling relation for finite-size systems with $d \geq d_c^+$ (52), but since Eq. 3.29 fails as well this assumption of the emergence of a system with $d \geq d_c^+$ seems rather implausible.

Another explanation that one may deliver is that Eq. 3.27 is indeed respected, but the order parameter chosen here does not provide the actual critical exponents of the system. Therefore, assuming that Eq. 3.27 holds and noticing that α and z are independent

of the chosen order parameter, the actual correlation length exponent ν should give

$$\nu = \frac{2}{z+1}. \tag{3.30}$$

Since for strong disorder $z \propto D$, $\nu \to 0$ as $D \to \infty$, which is an unlikely scenario.

4 Entanglement properties of the XX model with correlated disorder

This chapter provides calculations of the so-called Rényi entanglement entropy for the XX_{CD} model. The first section shows that the clean chain scaling function also holds for the XX_{CD} model (this result is published in (41)). Furthermore, the central charge is determined and plotted as a function of disorder strength. Higher-order corrections in the scaling of the entanglement entropy are considered in the second section.

4.1 Scaling function and the central charge

Entanglement measurements used to be a exclusive topic of quantum information studies. Recently, however, such measurements became popular in condensed matter physics (53, 54), mainly because it provides an insight on long-range correlations. The most used quantity for measuring entanglement in many-body systems is the so-called von Neumann entropy S_{vN}. Dividing the system in two complementary parts A and B of sizes x and $L - x$, respectively, S_{vN} is thus given by

$$S_{vN} = -Tr\rho_A \ln \rho_A, \tag{4.1}$$

where $\rho_A = Tr_B\rho$ is the reduced density matrix, i.e. the partial trace of the density matrix ρ over the subsystem B.

For every 1D clean critical system it is known that the leading scaling behavior of the entanglement entropy is logarithmic (55, 56), i.e.

$$S_{vN}(x) \sim \frac{c}{3} \ln(x), \tag{4.2}$$

where c is the so-called central charge. Entanglement measurements became so widespread because of their relation with the central charge, which is used for classifying the system. For instance, it is known that the XX model belongs to the universality class with $c = 1$. Recently, it has been found that the XX chain with uncorrelated disorder also exhibits a logarithmic scaling for the entanglement entropy, similar to Eq. 4.2 but with an effective central charge $c_{eff} = \ln 2$ instead. (57)

Eq. 4.2 describes well the scaling of the entanglement entropy in the limit of large systems. For numerical studies, though, finite-size corrections are important. Such

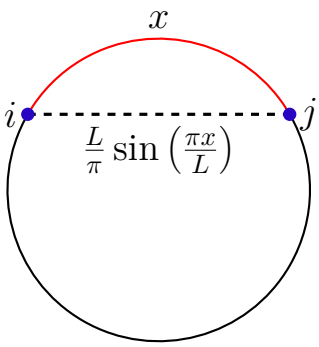

Figure 22 – Schematic of two spins i and j in a periodic spin chain of size L connected by the chord length (dashed line).

Source: By the author.

corrections can be found for the clean chain using conformal field theory (CFT) methods. Conformal invariance is the combination of rotational, translational and scale invariance. CFT approaches are best employed for two-dimensional (2D) classical critical points, or equivalently 1D quantum critical points.

Using CFT methods it has been found that finite-size effects diminish as one replaces x in Eq. 4.2 with the so-called chord length (58, 59)

$$f(x) = \frac{L}{\pi}\sin\left(\frac{\pi x}{L}\right). \tag{4.3}$$

The chord length is the line that connects two points of a circle, as Fig. 22 shows. Such scaling function, though, is not valid for random systems, since the introduction of disorder breaks conformal invariance. For instance, a conformally invariant model should have a dynamical exponent $z = 1$. However, for the XX_{CD} model Fig. 4 shows that $z \neq 1$ above D_C, while for the uncorrelated case $z \to \infty$.

Nevertheless, one can search for a scaling function for random chains by expanding $f(x)$ as a Fourier series, regarding periodic boundary conditions and symmetric properties. (60) For instance, it has been found that a good approximation for the scaling function of the uncorrelated random XX chain is

$$f(x) = \frac{L}{\pi}\sin\left(\frac{\pi x}{L}\right)\left[1 + b_1 \sin^2\left(\frac{\pi x}{L}\right)\right], \tag{4.4}$$

with $b_1 \approx 0.153$. (61) Conversely, for the XX_{CD} model it is shown in the following that a satisfactory scaling function is the clean system chord length, i.e. Eq. 4.3, even for $D > D_C$ where the necessary condition $z = 1$ is not obeyed.

Before showing the results for the scaling function of the XX_{CD} model, it is outlined the procedure to compute the entanglement entropy. Here it is investigated the so-called Rényi n-entropies, which are defined as

$$S_n = \frac{1}{1-n}\ln\left(Tr\rho_A^n\right). \tag{4.5}$$

Notice that in the limit $n \to 1$ Eq. 4.5 retrieves the von Neumann entropy (Eq. 4.1).

To calculate the entanglement entropy, one must first define the so-called correlation matrix

$$\mathcal{C}_i(x) = \begin{pmatrix} \left\langle c_i^\dagger c_i \right\rangle & \left\langle c_i^\dagger c_{i+1} \right\rangle & \cdots & \left\langle c_i^\dagger c_{i+x-1} \right\rangle \\ \left\langle c_{i+1}^\dagger c_i \right\rangle & \left\langle c_{i+1}^\dagger c_{i+1} \right\rangle & \cdots & \left\langle c_{i+1}^\dagger c_{i+x} \right\rangle \\ \vdots & \vdots & \ddots & \vdots \\ \left\langle c_{x-1+i}^\dagger c_i \right\rangle & \left\langle c_{x-1+i}^\dagger c_{i+1} \right\rangle & \cdots & \left\langle c_{x-1+i}^\dagger c_{x-1+i} \right\rangle \end{pmatrix}, \tag{4.6}$$

where the expectation values $\left\langle c_i^\dagger c_j \right\rangle$ are calculated from the eigenvectors of the Hamiltonian at criticality, as shown in Appendix A. Since the chain is periodic, the subsystem size x ranges from one to $L/2$. For each value of x one must diagonalize Eq. 4.6 and with the respective eigenvalues λ_i calculate the entanglement entropy, which is given by (62, 63)

$$S_n(x) = \frac{1}{1-n} \sum_{i=1}^{x} \ln\left[\lambda_i^n + (1-\lambda_i)^n\right], \tag{4.7}$$

and

$$S_{vN}(x) = -\sum_{i=1}^{x} \lambda_i \ln \lambda_i + (1-\lambda_i) \ln(1-\lambda_i) \tag{4.8}$$

for the von Neumann entropy ($n = 1$). Notice that, besides averaging over the number of disorder realizations, one can also average the entanglement entropy over the chain by varying the index i in Eq. 4.6.

From CFT methods it has been shown that the Rényi entanglement entropy of the clean chain scales as (58, 59)

$$S_n(x) = \frac{c}{6}\left(1 + \frac{1}{n}\right) \ln\left[f(x)\right] + a_0 + \textit{subleading terms}. \tag{4.9}$$

Cancelling out the constant a_0 by subtracting $S_n(L/2)$ from $S_n(x)$ and neglecting the subleading terms one can find

$$f(x) = \exp\left\{ \frac{6}{c} \frac{\left[S_n(x) - S_n\left(\frac{L}{2}\right)\right]}{\left(1 + \frac{1}{n}\right)} \right\}. \tag{4.10}$$

Thus, one can use Eq. 4.10 to determine the scaling function. Notice, however, that an input value for the central charge is required. This value is not known a priori for the XX_{CD} model, but one can consider a self-consistent approach. Such approach consists of fitting the central charge from the entanglement entropy calculations by assuming that the CFT scaling is valid. Then, using the fitted central charge as input in Eq. 4.10, one can show that the data is in good agreement with the proposed scaling.

Fig. 23 shows the entanglement entropy scaling function for the XX_{CD} model. The data were averaged over 10^5 disorder realizations, using disorder strength $D = 1.0$ and lattice size $L = 1024$. The entanglement entropy was computed for two values of n, namely

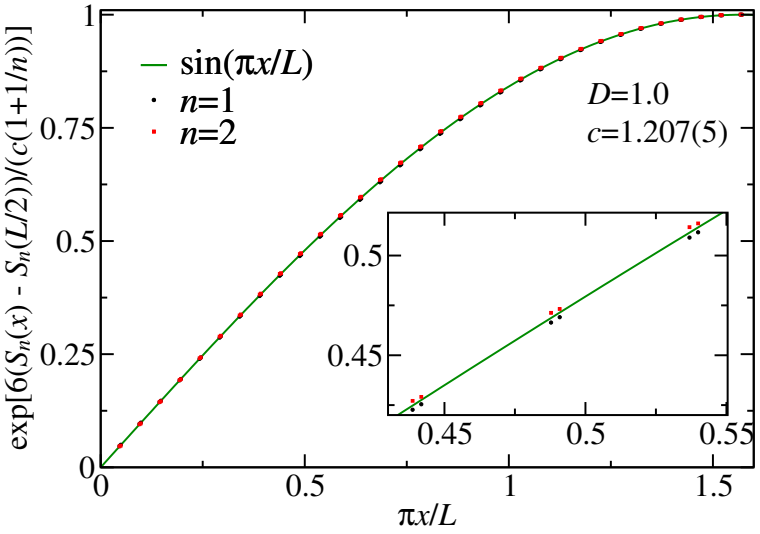

Figure 23 – Scaling function of the Rényi entanglement entropy $S_n(x)$ for $n = 1$ (black points) and $n = 2$ (red points), using $c = 1.20$ as the input central charge. The data were calculated for disorder strength $D = 1.0$ and chain size $L = 2^{10}$, averaging over 10^5 disorder realizations. The green line represents the expected scaling.

Source: GETELINA (41).

$n = 1$ and $n = 2$. Observe that the data are in good agreement with the chord length. For instance, the inset gives a closer look on the data, and it shows that the points are relatively close to the expected scaling. To give a quantitative estimate, the points were fitted to Eq. 4.4 and it was obtained $b_1 \approx 10^{-3}$, which is below the given precision. Thus, for the XX_{CD} model the expanded scaling function reduces to the chord length (Eq. 4.3) even though conformal invariance is lost.

After determining the scaling function of $S_n(x)$ for the XX_{CD} model, one can now find the central charge for various disorder strengths. Fig. 24 shows $S_n(x)$ for various n and two chain sizes L. It was also considered two values of disorder strength, namely $D = 1.0$ (top panel) and $D = 2.0$ (bottom panel). The data were averaged over 10^3 disorder realizations. Notice that all curves are parallel to the dashed lines, which give an estimate of the central charge. The value of c is also increasing as disorder gets stronger, contrasting with the uncorrelated disorder case where the effective central charge is universal. (57) Moreover, observe that an oscillatory behavior appears for $n \neq 1$ and the amplitude of the oscillations increases with n. These oscillations are due to higher-order corrections in the scaling of $S_n(x)$, which are considered in the next section.

Fig. 25 shows the central charge c as a function of disorder strength D. The central charge was fitted from $S_1(x)$ for two chain sizes L and within the region $1 \ll x \ll L$. Observe that for weak disorder ($D \leq D_C$) the central charge is equal to the clean chain value and for stronger disorder c increases monotonically with D. This result is shown here only for completeness, since it has already been reported. (9)

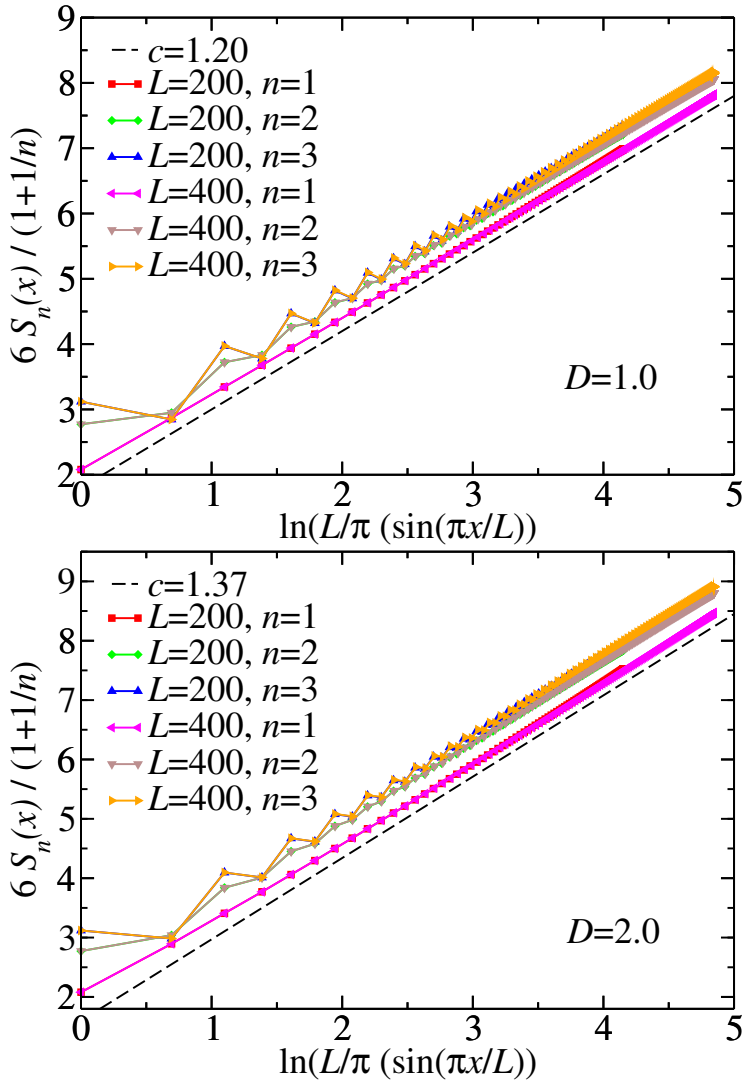

Figure 24 – Rényi entanglement entropy $S_n(x)$ for various n and two disorder strengths D, namely and chain sizes $L = 200$ and $L = 400$ for disorder strength $D = 1.0$ (top panel) and $D = 2.0$ (bottom panel). The data were averaged over 10^3 disorder realizations. The lines are guide to the eyes.

Source: GETELINA (41).

4.2 Higher-order corrections of the scaling

The previous section shows that the finite-size correction of the clean chain, viz. the chord length (Eq. 4.3), is also in good agreement with the XX_{CD} model. This result instigates an extension of the comparison with the clean chain by considering the subleading terms of the scaling. Up to first order, the CFT scaling of the Rényi entanglement entropy $S_n(x)$ is (64–66)

$$S_n(x) = a_0 + \frac{c}{6}\left(1 + \frac{1}{n}\right)\ln\left[f(x)\right] + a_2\frac{(-1)^x}{\left[f(x)\right]^{\frac{\phi}{n}}}. \tag{4.11}$$

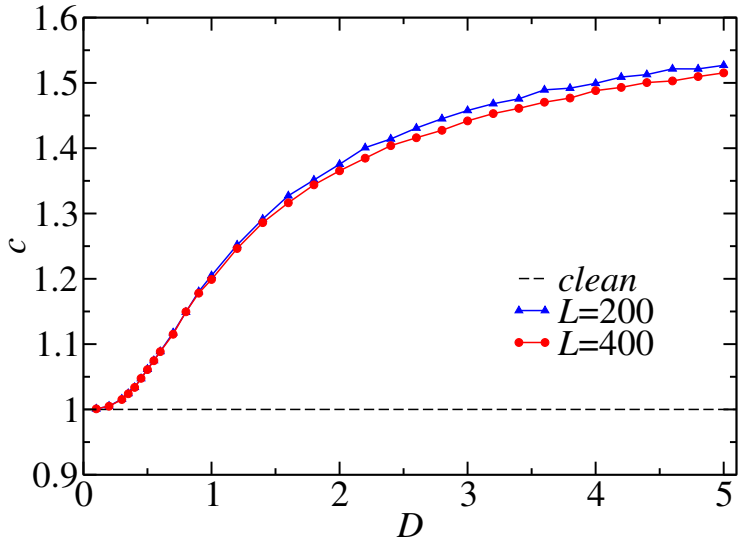

Figure 25 – Central charge c vs. disorder strength D fitted from the von Neumann entanglement entropy $S_1(x)$. The entanglement entropy was calculated for two chains with size $L = 200$ (blue triangles) and $L = 400$ (red circles), averaging over 10^3 disorder realizations for each value of D. The black dashed line is the clean chain central charge. Colored lines are guide to the eyes.

Source: By the author.

Therefore, in this section the data of $S_n(x)$ for the XX_{CD} model are fitted to Eq. 4.11. For every disorder strength and chain size, the entanglement entropy is averaged over 10^3 disorder realizations. The four parameters, namely a_0, c, a_2 and ϕ, are shown as a function of n, which varies from one to ten with a step of 0.1. To determine the parameters, the usual least-squares method is accompanied by a numerical procedure, as explained in Appendix E, because of the nonlinear parameter ϕ.

Fig. 26 shows the parameters a_0 and a_2 vs. n (panels (a) and (b), respectively) for various disorder strengths D. These parameters are not compared to clean chain. It is important, though, to observe that in panel (b) the parameter a_2 goes to zero as $n \to 1$ for each of the considered value of D. This result is in agreement with the clean chain behavior, where $a_2 = 0$ for $n = 1$.

Fig. 27 and Fig. 28 show the central charge c as a function of the parameter n for three disorder strengths, namely $D = 0.1$, $D = 1.0$ and $D = 2.0$. It is expected that the central charge is constant with respect to n. However, from Fig. 27 and Fig. 28 one can clearly observe that c varies with n. An explanation for such unexpected behavior are the finite-size effects. Thus, to test this hypothesis, the central charge is fitted for various chain sizes L. As the lattice size gets larger, one should observe the curves becoming more horizontal, which is indeed verified for every disorder strength. It is also expected that the curves approach each other with increasing L, which is not observed in Fig. 28. Another issue is that higher-order corrections should be considered as n increases. (66) However, this would make the fitting procedure even more difficult. In addition, the introduction of

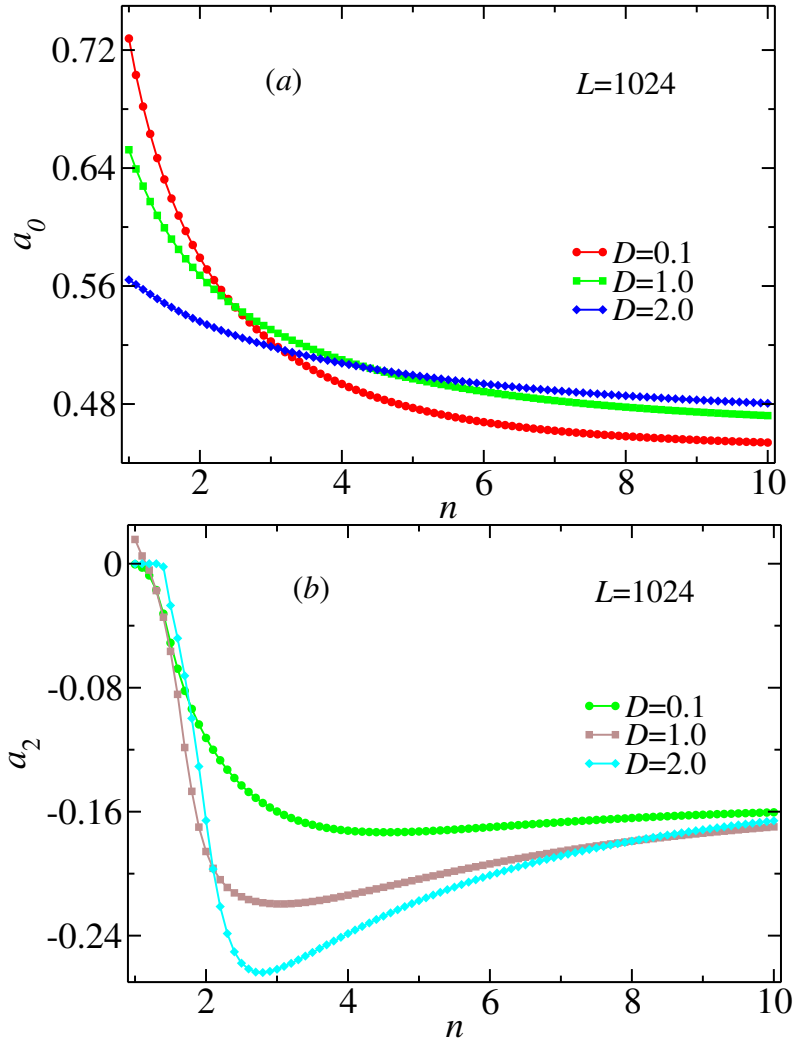

Figure 26 – The parameters a_0 and a_2 (see Eq. 4.9) vs. n (panels (a) and (b), respectively) for various disorder strengths D. The parameters were fitted from the average entanglement entropy $S_n(x)$, which was calculated for chain size $L = 1024$.

Source: By the author.

disorder may also require further corrections that cannot be predicted by CFT.

Lastly, Fig. 29* shows the exponent ϕ vs. the parameter n for disorder strength $D = 0.1$ and $D = 1.0$. For $D = 0.1$, notice that the curves become more horizontal as the chain size L is increased and they stay relatively close to the clean chain value. The region $n < 2$ is not reliable, since as $n \to 1$ the prefactor a_2 gets closer to zero and the subleading correction is irrelevant. One can also observe that the exponent ϕ changes with disorder, as for $D = 1.0$ it remains approximately close to three. The data for D=2.0 is not shown because the results were not satisfactory.

For completeness, Fig. 30 compares the data of $S_n(x)$ with the corresponding best fitting curve (dashed lines), which was obtained using Eq. 4.11. The inset gives a closer look

*Recall that the data are not continuous lines; the points were neglected for simplicity.

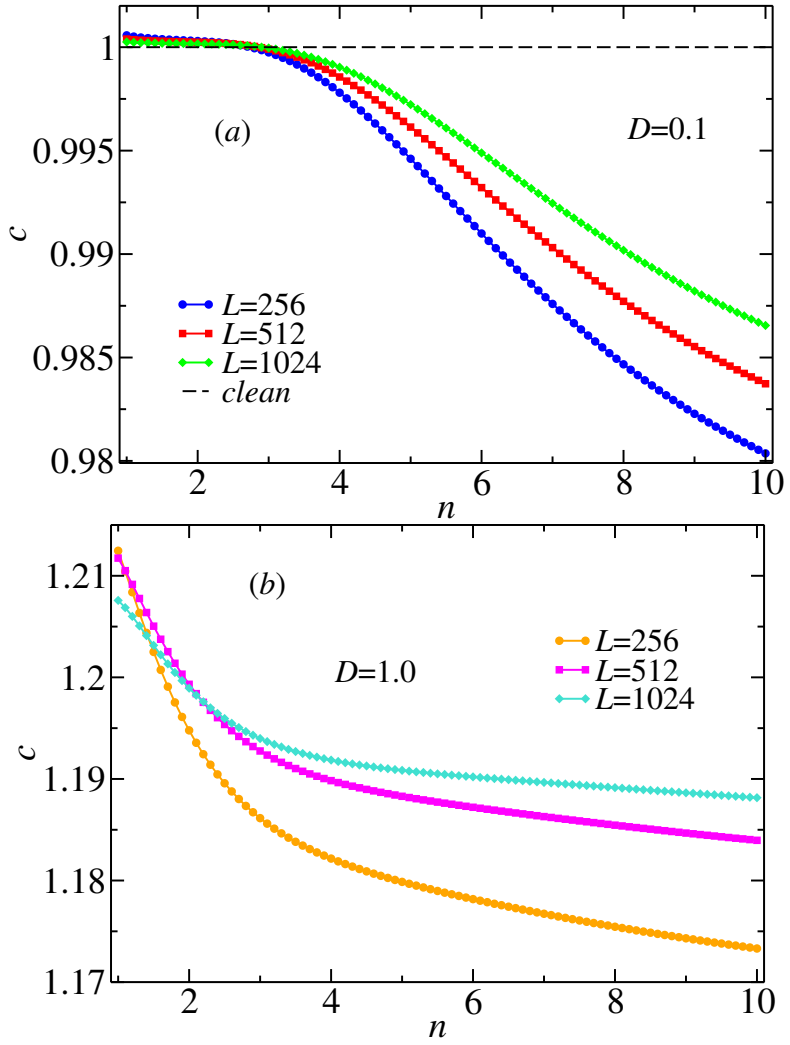

Figure 27 – Central charge c vs. the parameter n for disorder strength $D = 0.1$ (panel (a)) and $D = 1.0$ (panel (b)). The central charge was fitted from the average entanglement entropy $S_n(x)$, which was calculated for various chain sizes L. The dashed line in panel (a) is the clean chain central charge.

Source: By the author.

for $n = 3$ in the region $1 \ll x \ll L$. Notice that the fitted curves are in good agreement with the numerical data. As the parameter n increases, though, the difference between them becomes more significant. One can explain such discrepancy with the neglected higher-order corrections, which are required for greater n.

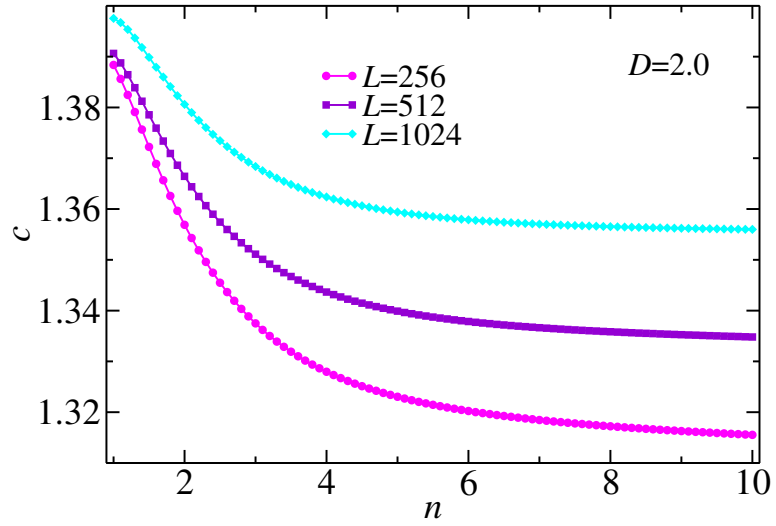

Figure 28 – Central charge c vs. the parameter n for disorder strength $D = 2.0$. The central charge was fitted from the average entanglement entropy $S_n(x)$, which was calculated for various chain sizes L.

Source: By the author.

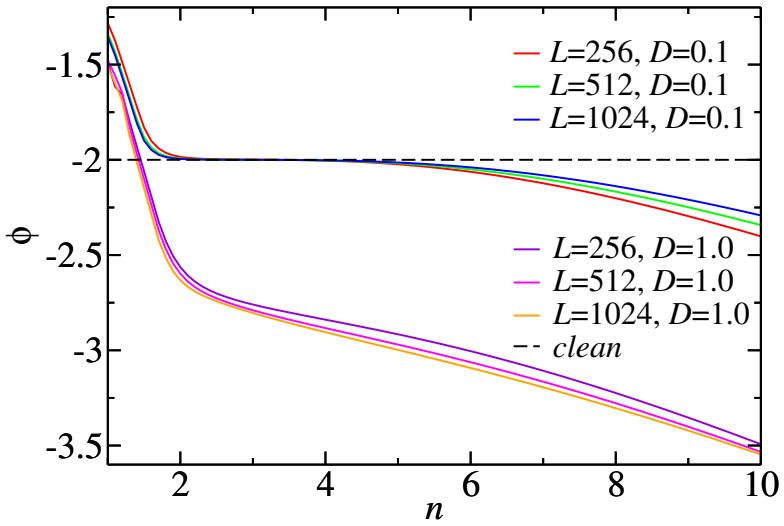

Figure 29 – The exponent ϕ vs. the parameter n for disorder strengths $D = 0.1$ and $D = 1.0$. The exponent was fitted from the average entanglement entropy $S_n(x)$, which was calculated for various chain sizes L. The dashed line is the clean chain exponent.

Source: By the author.

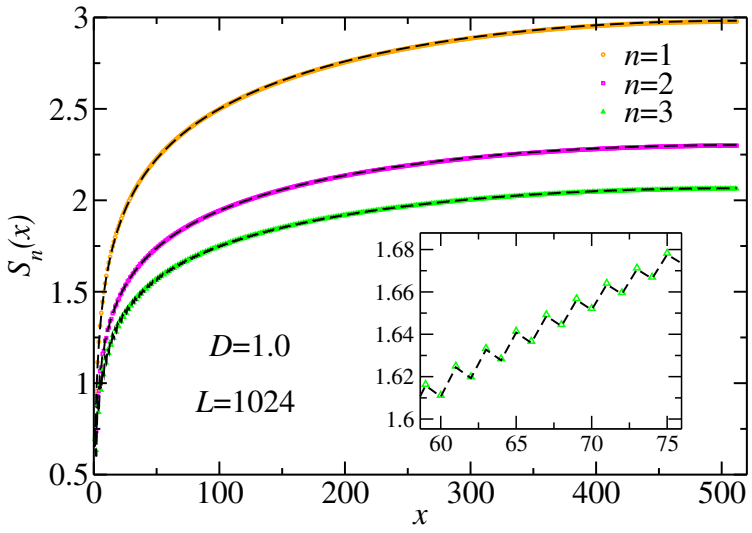

Figure 30 – Rényi entanglement entropy $S_n(x)$ for various n, disorder strength $D = 1.0$ and lattice size $L = 1024$. The data were averaged over 10^3 disorder realizations. The dashed lines were calculated from Eq. 4.11 using the best fitting values of the parameters.

Source: By the author.

5 Conclusion

The complete set of critical exponents of the XX_{CD} model, namely $\{\alpha, \beta, \gamma, \delta, \eta, \nu\}$, has been determined. It has been found that most of them are universal, i.e. disorder independent, and equal to the clean chain exponent. The only exception is the anomalous dimension η. Besides the usual set of critical exponents, the so-called critical dynamical exponent z was also determined. It has been shown that z increases monotonically with disorder strength D and is equal to the clean value for $D \leq D_C \approx 0.3$. Thus, one may conclude that for weak disorder (i.e. below D_C) the clean critical point is preserved. As disorder gets stronger, though, the system falls into a family of finite-disorder critical points, each of them characterized by a unique z.

However, this disorder-dependent dynamical exponent results in unreliable values for the anomalous dimension η. For instance, for sufficiently strong disorder, $\eta < 0$ which is not acceptable. Such negative values of η are obtained from the premise that, for quantum critical systems, one should replace d with $d + z$. As another consequence of this substitution, two scaling relations, viz. hyperscaling and Fisher's scaling relations, do not hold for disorder strength above D_C. The other two scaling relations that do not involve dimensionality are respected even for $D > D_C$.

There is not much literature available about the validation of the hyperscaling and Fisher's scaling relations for random quantum phase transitions. Thus, it would be interesting to test such relations for other models. However, a more appropriate procedure would be to derive those relations from the beginning for quantum critical points and see where the introduction of disorder may interfere. As shown here, just replacing d for $d + z$ is not sufficient to validate the scaling relations. In addition, the failure of two scaling relations may indicate that there are more than two independent critical exponents.

The observed numerical results strongly suggest that the critical exponents are disorder independent (except for η and z). However, from numerical studies alone it is not possible to prove this independence. This study should be accompanied with theoretical approaches, such as the renormalization group. It is not known, though, how to extract all quantities of interest from the renormalization group of finite-disorder critical points; this method is best employed for infinite-randomness critical points, such as the XX model with uncorrelated disorder.

Alongside the usual study of the critical behavior, it has also been performed calculations of the Rényi entanglement entropy. Surprisingly, it has been found that the leading scaling behavior in Eq. 4.9 and the finite-size correction of the clean system

(namely the chord length) are in good agreement for the XX_{CD} model as well. This result is intriguing because the entanglement entropy scaling and the chord length are derived from conformal field theory methods and a necessary condition for conformal invariance is that $z = 1$, which does not occur for $D > D_C$. Thus, this result suggests that the logarithmic scaling in Eq. 4.9 and the chord length may be derived from a more general assumption than conformal invariance, which may also include random systems.

Furthermore, it has been found that the corresponding central charge c increases monotonically with disorder strength D, contrasting with the uncorrelated disorder case where the effective central charge is universal. It has also been shown the central charge as a function of the parameter n of the Rényi entanglement entropy. It was expected that c and the exponent ϕ (introduced in the first-order correction) were universal, i.e. independent of n. However, this independence was not verified, mostly because of finite-size effects. Nevertheless, one could obtain better results if chains with open boundaries were considered instead. (67) Moreover, to achieve a deeper understanding of the entanglement properties of the XX_{CD} model one should consider a study of the real-space entanglement spectrum. (68)

The next step is to investigate other systems under correlated disorder and check if the same behavior occurs. Indeed, the correlated disorder XXZ spin-1/2 chain has been investigated and it turns out that it behaves similarly to the XX_{CD} model. (41) However, renormalization group calculations show that this behavior for the XXZ model is due to finite-size effects; for sufficiently large lattices the uncorrelated case is retrieved. Conversely, for the XX_{CD} model there is no such crossover length, although it has not been proven here.

References

1 NGUYEN, T. N.; LEE, P. A.; LOYE, H.-C. zur. Design of a random quantum spin chain paramagnet: Sr3CuPt0.5Ir0.5O6. *Science*, v. 271, n. 5248, p. 489–491, 1996.

2 IRONS, S. H. et al. ac susceptibility of Sr3CuPtIrO6 : a magnetic system with competing interactions and dimensionality. *Physical Review B*, v. 61, n. 17, p. 594–600, 2000.

3 KOTESWARARAO, B. et al. Doping effects in the coupled, two-leg spin ladder BiCu(2)PO(6). *Journal of Physics:* condensed matter, v. 22, n. 3, p. 035601, 2010.

4 MA, S.-k.; DASGUPTA, C.; HU, C.-k. Random antiferromagnetic chain. *Physical Review Letters*, v. 43, n. 19, p. 1434–1437, 1979.

5 FISHER, D. Critical behavior of random transverse-field Ising spin chains. *Physical Review B*, v. 51, n. 10, p. 6411–6461, 1995.

6 IGLÓI, F.; MONTHUS, C. Strong disorder RG approach of random systems. *Physics Reports*, v. 412, n. 5-6, p. 277–431, 2005.

7 DOTY, C. A.; FISHER, D. S. Effects of quenched disorder on spin-1/2 quantum XXZ chains. *Physical Review B*, v. 45, n. 5, p. 2167–2179, 1992.

8 BINOSI, D. et al. Increasing entanglement through engineered disorder in the random Ising chain. *Physical Review B*, v. 76, n. 14, p. 1–4, 2007.

9 HOYOS, J. A. et al. Protecting clean critical points by local disorder correlations. *Europhysics Letters*, v. 93, n. 3, p. 30004, 2011.

10 VOJTA, T. Quantum phase transitions in electronic systems. *Annalen der Physik*, v. 9, n. 6, p. 403–440, 2000.

11 VOJTA, M. Quantum phase transitions. *Reports on Progress in Physics*, v. 66, n. 12, p. 2069–2110, 2003.

12 VOJTA, T. Rare region effects at classical, quantum and nonequilibrium phase transitions. *Journal of Physics A:* mathematical and general, v. 39, n. 22, p. R143–R205, 2006.

13 SONDHI, S. L.; SHAHAR, D. Continuous quantum phase transitions. *Reviews of Modern Physics*, v. 69, n. 1, p. 315–333, 1997.

14 SACHDEV, S. *Quantum phase transitions*. Cambridge: Cambridge University Press, 2011.

15 LÖHNEYSEN, H. et al. Non-Fermi-liquid behavior in a heavy-fermion alloy at a magnetic instability. *Physical Review Letters*, v. 72, n. 20, p. 3262–3265, 1994.

16 BITKO, D.; ROSENBAUM, T.; AEPPLI, G. Quantum critical behavior for a model magnet. *Physical Review Letters*, v. 77, n. 5, p. 940–943, 1996.

17 NEUMANN, M. et al. Bilayer 3He: a simple two-dimensional heavy-fermion system with quantum criticality. *Science*, v. 317, n. 5843, p. 1356–9, 2007.

18 GOLDENFELD, N. *Lectures on phase transitions and the renormalization group.* Reading: Perseus Books, 1992.

19 REICHL, L. E. *A modern course in statistical physics.* New York: John Wiley & Sons, 1998.

20 CARDY, J. *Scaling and renormalization in statistical physics.* Cambridge: Cambridge University Press, 1996.

21 SUZUKI, M. Relationship between d-dimensional quantal spin systems and (d+1)-dimensional Ising systems: equivalence, critical exponents and systematic approximants of the partition function and spin correlations. *Progress of Theoretical Physics*, v. 56, n. 5, p. 1454–1469, 1976.

22 IMRY, Y. Random-field instability of the ordered state of continuous symmetry. *Physical Review Letters*, v. 35, n. 21, p. 1399–1401, 1975.

23 FISHER, D. Random antiferromagnetic quantum spin chains. *Physical Review B*, v. 50, n. 6, p. 3799–3821, 1994.

24 MACDIARMID, A. G. et al. Polyaniline: a new concept in conducting polymers. *Synthetic Metals*, v. 18, n. 1-3, p. 285–290, 1987.

25 DUNLAP, D. H.; WU, H.-L.; PHILLIPS, P. W. Absence of localization in a random-dimer model. *Physical Review Letters*, v. 65, n. 1, p. 88–91, 1990.

26 WU, H.-L.; PHILLIPS, P. Polyaniline is a random-dimer model: a new transport mechanism for conducting polymers. *Physical Review Letters*, v. 66, n. 10, p. 1366–1369, 1991.

27 LIEB, E.; SCHULTZ, T.; MATTIS, D. Two soluble models of an antiferromagnetic chain. *Annals of Physics*, v. 16, n. 3, p. 407–466, 1961.

28 PFEUTY, P. An exact result for the 1D random Ising model in a transverse field. *Physics Letters A*, v. 72, n. 3, p. 245–246, 1979.

29 HARRIS, A. Effect of random defects on the critical behaviour of Ising models. *Journal of Physics C:* solid state physics, v. 7, p. 1671–1692, 1974.

30 VOJTA, T.; HOYOS, J. A. Criticality and quenched disorder: Harris criterion versus rare regions. *Physical Review Letters*, v. 112, n. 7, p. 075702, 2014.

31 AHARONY, A.; HARRIS, A. B. Absence of self-averaging and universal fluctuations in random systems near critical points. *Physical Review Letters*, v. 77, n. 18, p. 3700–3703, 1996.

32 WISEMAN, S.; DOMANY, E. Lack of self-averaging in critical disordered systems. *Physical Review E*, v. 52, n. 4, p. 3469–3484, 1995.

33 WISEMAN, S.; DOMANY, E. Self-averaging, distribution of pseudocritical temperatures, and finite size scaling in critical disordered systems. *Physical Review E*, v. 58, n. 3, p. 2938–2951, 1998.

34 WISEMAN, S.; DOMANY, E. Finite-size scaling and lack of self-averaging in critical disordered systems. *Physical Review Letters*, v. 81, n. 1, p. 22–25, 1998.

35 WEINRIB, A.; HALPERIN, B. I. Critical phenomena in systems with long-range-correlated quenched disorder. *Physical Review B*, v. 27, n. 1, p. 413–427, 1983.

36 YAO, D.-X. et al. Quantum phase transitions in disordered dimerized quantum spin models and the Harris criterion. *Physical Review B*, v. 82, n. 17, p. 172409, 2010.

37 FISHER, M.; BARBER, M. Scaling theory for finite-size effects in the critical region. *Physical Review Letters*, v. 28, n. 23, p. 1516–1519, 1972.

38 CHAYES, J. et al. Finite-size scaling and correlation lengths for disordered systems. *Physical Review Letters*, v. 57, n. 24, p. 2999–3002, 1986.

39 LAFLORENCIE, N. et al. Crossover effects in the random-exchange spin-12 antiferromagnetic chain. *Physical Review B*, v. 70, n. 5, p. 54430, 2004.

40 HOYOS, J. A. et al. Correlation amplitude and entanglement entropy in random spin chains. *Physical Review B*, v. 76, n. 17, p. 174425, 2007.

41 GETELINA, J. C.; ALCARAZ, F. C.; HOYOS, J. A. Entanglement properties of correlated random spin chains and similarities with conformally invariant systems. *Physical Review B*, v. 93, n. 4, p. 045136, 2016.

42 HENELIUS, P.; GIRVIN, S. Numerical study of the random dimerized XX spin-1/2 chain. *Physical Review B*, v. 57, n. 18, 1998.

43 HIDA, K. Crossover between the Haldane-gap phase and the dimer phase in the spin-1/2 alternating Heisenberg chain. *Physical Review B*, v. 45, n. 5, p. 2207–2212, 1992.

44 HYMAN, R. et al. Random bonds and topological stability in gapped quantum spin chains. *Physical Review Letters*, v. 76, n. 5, p. 839–842, 1996.

45 HALDANE, F. D. M. Nonlinear field theory of large-spin Heisenberg antiferromagnets: semiclassically quantized solitons of the one-dimensional easy-axis Néel state. *Physical Review Letters*, v. 50, n. 15, p. 1153–1156, 1983.

46 HALDANE, F. Continuum dynamics of the 1-D Heisenberg antiferromagnet: Identification with the O(3) nonlinear sigma model. *Physics Letters A*, v. 93, n. 9, p. 464–468, 1983.

47 GRIFFITHS, R. B. Nonanalytic behavior above the critical point in a random Ising ferromagnet. *Physical Review Letters*, v. 23, n. 1, p. 17–19, 1969.

48 GUO, M.; BHATT, R. N.; HUSE, D. A. Quantum Griffiths singularities in the transverse-field Ising spin glass. *Physical Review B*, v. 54, n. 5, p. 3336–3342, 1996.

49 RIEGER, H.; YOUNG, A. P. Griffiths singularities in the disordered phase of a quantum Ising spin glass. *Physical Review B*, v. 54, n. 5, p. 3328–3335, 1996.

50 VOJTA, T.; SKNEPNEK, R. Critical points and quenched disorder: from Harris criterion to rare regions and smearing. *Physica Status Solidi B*, v. 241, n. 9, p. 2118–2127, 2004.

51 BERCHE, B.; KENNA, R.; WALTER, J.-C. Hyperscaling above the upper critical dimension. *Nuclear Physics B*, v. 865, n. 1, p. 115–132, 2012.

52 KENNA, R.; BERCHE, B. Fisher's scaling relation above the upper critical dimension. *Europhysics Letters*, v. 105, n. 2, p. 26005, 2014.

53 AMICO, L.; OSTERLOH, A.; VEDRAL, V. Entanglement in many-body systems. *Reviews of Modern Physics*, v. 80, n. 2, p. 517–576, 2008.

54 REFAEL, G.; MOORE, J. E. Criticality and entanglement in random quantum systems. *Journal of Physics A:* mathematical and theoretical, v. 42, n. 50, p. 504010, 2009.

55 VIDAL, G. et al. Entanglement in quantum critical phenomena. *Physical Review Letters*, v. 90, n. 22, p. 227902, 2003.

56 KOREPIN, V. Universality of entropy scaling in one dimensional gapless models. *Physical Review Letters*, v. 92, n. 9, p. 96402, 2004.

57 REFAEL, G.; MOORE, J. Entanglement entropy of random quantum critical points in one dimension. *Physical Review Letters*, v. 93, n. 26, p. 260602, 2004.

58 CALABRESE, P.; CARDY, J. Entanglement entropy and quantum field theory. *Journal of Statistical Mechanics:* theory and experiment, v. 2004, n. 06, p. P06002, 2004.

59 CALABRESE, P.; CARDY, J. Entanglement entropy and conformal field theory. *Journal of Physics A:* mathematical and theoretical, v. 42, n. 50, p. 504005, 2009.

60 IGLÓI, F.; LIN, Y.-C. Finite-size scaling of the entanglement entropy of the quantum Ising chain with homogeneous, periodically modulated and random couplings. *Journal of Statistical Mechanics:* theory and experiment, v. 2008, n. 06, p. P06004, 2008.

61 FAGOTTI, M.; CALABRESE, P.; MOORE, J. E. Entanglement spectrum of random-singlet quantum critical points. *Physical Review B*, v. 83, n. 4, p. 1–11, 2011.

62 PESCHEL, I. Calculation of reduced density matrices from correlation functions. *Journal of Physics A:* mathematical and general, v. 36, n. 14, p. L205–L208, 2003.

63 LAFLORENCIE, N. Scaling of entanglement entropy in the random singlet phase. *Physical Review B*, v. 72, n. 14, p. 140408, 2005.

64 XAVIER, J. C.; ALCARAZ, F. C. Finite-size corrections of the entanglement entropy of critical quantum chains. *Physical Review B*, v. 85, n. 2, p. 24418, 2012.

65 CALABRESE, P. et al. Parity effects in the scaling of block entanglement in gapless spin chains. *Physical Review Letters*, v. 104, n. 9, p. 95701, 2010.

66 CALABRESE, P.; ESSLER, F. H. L. Universal corrections to scaling for block entanglement in spin-1/2 XX chains. *Journal of Statistical Mechanics:* theory and experiment, v. 2010, n. 08, p. P08029, 2010.

67 D'EMIDIO, J.; BLOCK, M. S.; KAUL, R. K. Rényi entanglement entropy of critical SU(N) spin chains. *Physical Review B*, v. 92, n. 5, p. 054411, 2015.

68 LAFLORENCIE, N.; RACHEL, S. Spin-resolved entanglement spectroscopy of critical spin chains and Luttinger liquids. *Journal of Statistical Mechanics:* theory and experiment, v. 2014, n. 11, p. P11013, 2014.

69 FETTER, A. L.; WALECKA, J. D. *Quantum theory of many-particle systems.* Mineola: Dover, 2003.

70 MCCOY, B. Spin correlation functions of the X-Y model. *Physical Review*, v. 173, n. 2, p. 531–541, 1968.

APPENDIX A – Some properties of the Hamiltonian

This appendix outlines the procedure to write the Hamiltonian in its diagonal basis. This is a necessary step to evaluate expectation values such as $\left\langle c_i^\dagger c_j \right\rangle$, which are related to some of the quantities of interest, e.g. the correlation function. Some matrix properties that simplify calculations are also presented.

The matrix representation of H in the old basis is

$$H = \boldsymbol{c}^\dagger M \boldsymbol{c}, \tag{A.1}$$

where M is the matrix in Eq. 2.20 and $\boldsymbol{c}^\dagger$ ($\boldsymbol{c}$) is a row (column) vector with the L fermionic operators, i.e.

$$\boldsymbol{c} = \begin{pmatrix} c_1 \\ c_2 \\ \vdots \\ c_L \end{pmatrix}, \qquad \boldsymbol{c}^\dagger = \begin{pmatrix} c_1^\dagger & c_2^\dagger & \cdots & c_L^\dagger \end{pmatrix}. \tag{A.2}$$

It is desired to rewrite the Hamiltonian in the diagonal basis, i.e.

$$H = \boldsymbol{\eta}^\dagger D \boldsymbol{\eta}, \tag{A.3}$$

where $\boldsymbol{\eta}^\dagger$ and $\boldsymbol{\eta}$ are the diagonal fermionic operators and

$$D = \begin{pmatrix} \lambda_1 & 0 & \cdots & 0 \\ 0 & \lambda_2 & 0 & \vdots \\ \vdots & \vdots & \ddots & 0 \\ 0 & \cdots & 0 & \lambda_L \end{pmatrix}, \tag{A.4}$$

where λ_i is the i-th eigenvalue of M with $\lambda_1 < \lambda_2 < \cdots < \lambda_L$.

The change of basis above is called a similarity transformation, in which the eigenvalues of the matrix are unaltered. This transformation can be represented in general as

$$D = V^{-1} M V, \tag{A.5}$$

where V (V^{-1}) is the (inverse) transformation matrix to be determined. For hermitian matrices, such as M, one can show that V is the matrix with the eigenvectors $\boldsymbol{v}$ of M

stored column wise, i.e.,

$$\begin{aligned} V &= \begin{pmatrix} v_{1,1} & v_{1,2} & \cdots & v_{1,L} \\ v_{2,1} & v_{2,2} & \cdots & v_{2,L} \\ \vdots & \vdots & \vdots & \vdots \\ v_{L,1} & v_{L,2} & \cdots & v_{L,L} \end{pmatrix}, \\ &= \begin{bmatrix} \boldsymbol{v}_1 & \boldsymbol{v}_2 & \cdots & \boldsymbol{v}_L \end{bmatrix}. \end{aligned} \tag{A.6}$$

To show that the matrix above satisfies the transformation notice that

$$\begin{aligned} MV &= M \begin{bmatrix} \boldsymbol{v}_1 & \boldsymbol{v}_2 & \cdots & \boldsymbol{v}_L \end{bmatrix}, \\ &= \begin{bmatrix} \lambda_1 \boldsymbol{v}_1 & \lambda_2 \boldsymbol{v}_2 & \cdots & \lambda_L \boldsymbol{v}_L \end{bmatrix}. \end{aligned} \tag{A.7}$$

Since the eigenvectors matrix V is unitary (or orthogonal, since $\boldsymbol{v} \in \mathbb{R}$), $V^{-1} = V^T$ and $V^T V = V V^T = I$, where V^T is the transpose of V and I is the identity matrix. Thus,

$$\begin{aligned} V^T M V &= \begin{bmatrix} \boldsymbol{v}_1 \\ \boldsymbol{v}_2 \\ \vdots \\ \boldsymbol{v}_L \end{bmatrix} \begin{bmatrix} \lambda_1 \boldsymbol{v}_1 & \lambda_2 \boldsymbol{v}_2 & \cdots & \lambda_L \boldsymbol{v}_L \end{bmatrix}, \\ &= \begin{pmatrix} \lambda_1 & 0 & \cdots & 0 \\ 0 & \lambda_2 & 0 & \vdots \\ \vdots & \vdots & \ddots & 0 \\ 0 & \cdots & 0 & \lambda_L \end{pmatrix}, \end{aligned} \tag{A.8}$$

which is indeed the matrix D.

Using the transformation in Eq. A.5 and comparing Eq. A.1 with Eq. A.3 one finds that $\boldsymbol{c}^\dagger M \mathbf{c} = \boldsymbol{\eta}^\dagger V^T M V \boldsymbol{\eta}$. Therefore, the i-th component of $\boldsymbol{c}^\dagger$ and $\boldsymbol{c}$ is, respectively,

$$c_i^\dagger = \sum_{j=1}^{L} \eta_j^\dagger v_{i,,j}, \tag{A.9}$$

$$c_i = \sum_{j=1}^{L} \eta_j v_{i,j}. \tag{A.10}$$

The expectation value $\left\langle c_i^\dagger c_j \right\rangle$ is evaluated on the ground state $|GS\rangle$ of the system. The ground state is constructed by creating fermions up to the Fermi level $\mu = 0$, i.e.

$$|GS\rangle = \prod_{i=1}^{\frac{L}{2}} \eta_i^\dagger \left|0\right\rangle, \tag{A.11}$$

where $|0\rangle$ is the vacuum. Hence, the expectation value is

$$\left\langle c_i^\dagger c_j \right\rangle = \left\langle \left(\sum_{k=1}^{L} \eta_k^\dagger v_{i,k} \right) \left(\sum_{m=1}^{L} \eta_m v_{j,m} \right) \right\rangle. \tag{A.12}$$

The operator η_m will first act on the ground state and annihilate a preexisting fermion. Therefore $m < L/2+1$, which can be represented as a step function $\theta\left(\frac{L}{2} - m\right)$. The second operator $\eta_k^\dagger$ will create a fermion in a vacancy. However, if $k \neq m$ the right eigenstate will be different than the left one, which will result $\left\langle c_i^\dagger c_j \right\rangle = 0$. Thus, a Kronecker delta ($\delta_{k,m}$) is also needed, yielding

$$\begin{aligned} \left\langle c_i^\dagger c_j \right\rangle &= \sum_{k=1}^{L}\sum_{m=1}^{L} v_{i,k} v_{j,m} \theta\left(\frac{L}{2} - m\right) \delta_{k,m}, \\ &= \sum_{k=1}^{\frac{L}{2}} v_{i,k} v_{j,k}. \end{aligned} \tag{A.13}$$

Notice that the interchange between i and j do not change the result, i.e. $\left\langle c_i^\dagger c_j \right\rangle = \left\langle \left(c_i^\dagger c_j\right)^\dagger \right\rangle$.

As it turns out, the eigenvectors matrix V has a property that results in $\left\langle c_i^\dagger c_j \right\rangle = 0$ whenever $i + j$ is even. One can check from V that

$$v_{i,,j} = (-1)^{i-j}\, v_{i,L-j+1}. \tag{A.14}$$

Moreover, the orthonormality condition of eigenvectors requires that

$$\sum_{k=1}^{L} v_{i,k} v_{j,k} = \delta_{i,j}. \tag{A.15}$$

Rewriting the relation above using Eq. A.14 gives

$$\left[1 + (-1)^{i+j}\right] \sum_{k=1}^{\frac{L}{2}} v_{i,k} v_{j,k} = \delta_{i,j}. \tag{A.16}$$

If $i = j$ the equation above gives $\left\langle c_i^\dagger c_i \right\rangle = \sum_{k=1}^{\frac{L}{2}} v_{i,k} v_{j,k} = 1/2$. For $i \neq j$ the right side of the equation is zero, which means that one of the multiplying terms on the left side must be zero as well. If $i + j$ is even the term within brackets equals two, which implies that the summation is zero, i.e. $\left\langle c_i^\dagger c_j \right\rangle = 0$ for $i + j$ even. Thus it is only necessary to evaluate $\left\langle c_i^\dagger c_j \right\rangle$ when $i \neq j$ and their sum gives an odd number.

Besides using this property one can further reduce computation time by diagonalizing the squared Hamiltonian H^2 instead of H, as discussed in Chapter 2. Let V_{odd} and V_{even} be the eigenvector matrices of H^2_{odd} and H^2_{even}, respectively. The procedure to retrieve the eigenvector matrix V of H from the two block matrices is straightforward: Insert the entries of V_{odd} and V_{even} in the odd and even lines of V, respectively; i.e. $v_{2i-1} = v_i^{odd}/\sqrt{2}$ and $v_{2i} = v_i^{even}/\sqrt{2}$. The entries must be divided by $\sqrt{2}$ because the program gives normalized eigenvectors. Furthermore, the given eigenvectors are stored column wise in crescent order. Thus, the combination of the first column of V_{odd} and V_{even} corresponds to either the $L/2$-th or $L/2 + 1$-th column of V. To check whether the i-th eigenvalue is positive or negative one can compute $\lambda_i = \boldsymbol{v}_i H \boldsymbol{v}_i$. Using Eq. A.13 one can obtain right after the opposite eigenvector.

APPENDIX B – Numerical instabilities

This appendix contains a discussion about the diagonalization of the squared Hamiltonian H^2, which may lead to imprecise eigenvalues and eigenvectors. It is shown that using H^2 is reliable for $D \leq 2.0$; for stronger disorder one should stay with the original Hamiltonian H.

To check whether the i-th eigenvalue λ_i given by the program is reliable, one can compute the corresponding relative error σ_i, which is defined as

$$\sigma_i = 1 - \frac{\lambda_i'}{\lambda_i}, \tag{B.1}$$

where $\lambda_i' = \boldsymbol{v}_i H \boldsymbol{v}_i$ is the expectation value and $\boldsymbol{v}_i$ is the i-th column of the eigenvector matrix V.

Fig. 31 shows σ_i vs. λ_i for various chain sizes L and disorder strength $D = 5.0$ (panel (a)) and also for various D and $L = 2^{10}$ (panel (b)). The eigenvalues were calculated from H and H^2, averaging over 10^3 disorder realizations. The dashed line delimits the desired precision; only the points below it are reliable. Notice that the number of imprecise eigenvalues rises as disorder and chain size increase. Furthermore, the eigenvalues of H^2 (non-filled symbols) are clearly less reliable than those of H (filled symbols).

Imprecise eigenvalues (or eigenvectors) may generate misleading results for the quantities of interest. For instance, it has been observed that the correlation function violated the expected scaling when calculated using H^2 eigenvectors for $D \geq 3.0$ and $L = 2^9$. Therefore, according to Fig. 31, one can say that squaring the Hamiltonian is a reliable procedure only for disorder strength $D \leq 2.0$.

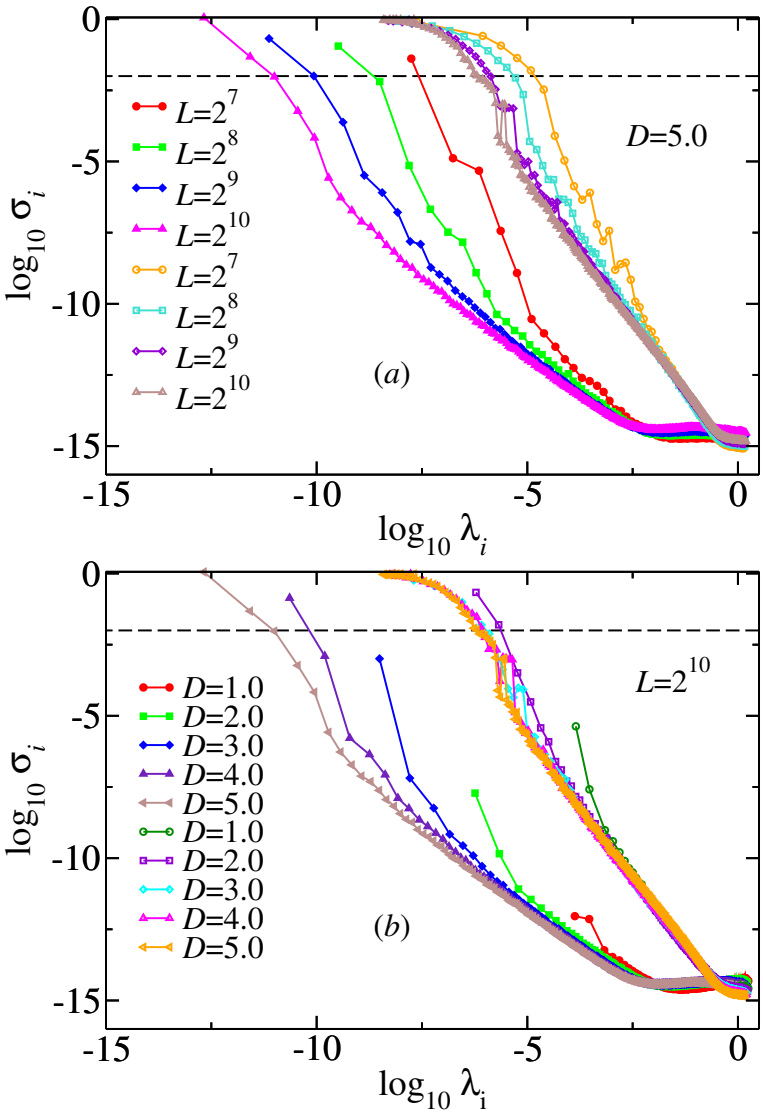

Figure 31 – Relative error σ_i vs. the eigenvalue λ_i for (a) various chain size L and disorder strength $D = 5.0$ and (b) several disorder strengths and chain size $L = 2^{10}$. The eigenvalues were averaged over 10^3 disorder realizations. Eigenvalues calculated from H and H^2 are represented as filled and open symbols, respectively. The dashed line delimits the desired precision. Colored lines are guide to the eyes.

Source: By the author.

APPENDIX C – Expressions for the specific heat and the magnetic susceptibility

This appendix shows how to derive expressions for the specific heat and magnetic susceptibility using the statistical mechanics approach.

From the canonical ensemble formalism, the specific heat C is defined as (19)

$$C = -T\left(\frac{\partial^2 f}{\partial T^2}\right), \tag{C.1}$$

where f is the free energy density and T is the temperature. The definition of the magnetic susceptibility χ is similar to the specific heat, except that the derivative is with respect to an external magnetic field B, i.e.

$$\chi = -\left(\frac{\partial^2 f}{\partial B^2}\right)_{B=0}, \tag{C.2}$$

where the derivative is taken in the limit $B \to 0$.

The introduction of the field B changes the Hamiltonian of the system, since one must also considered the interaction of the spins with the field. Thus, the new Hamiltonian is defined as $H' = H + H_B$, where

$$H_B = B\sum_{i=1}^{L} S_i^z \tag{C.3}$$

is the term that comprises the spin-field interactions, considering that B is constant and points in the z-direction.

To compute the free energy it is easier to write the new Hamiltonian H' in its diagonal basis, as shown in Appendix A for H. To write H_B in the same basis one can use Eq. 2.10 to map S_i^z to the fermionic operators $c^\dagger$ and c. Furthermore, according to Eq. A.9 and Eq. A.10, one can find that

$$\begin{aligned}\sum_{i=1}^{L} c_i^\dagger c_i &= \sum_{i=1}^{L}\left(\sum_{j=1}^{L}\eta_j^\dagger v_{i,j}\right)\left(\sum_{k=1}^{L}\eta_k v_{i,k}\right), \\ &= \sum_{j=1}^{L}\sum_{k=1}^{L}\eta_j^\dagger\eta_k\left(\sum_{i=1}^{L} v_{i,j}v_{i,k}\right).\end{aligned} \tag{C.4}$$

Thus, since the eigenvectors are orthogonal (i.e. $\sum_{i=1}^{L} v_{ij}v_{ik} = \delta_{j,k}$), $\sum_{i=1}^{L} c_i^\dagger c_i = \sum_{i=1}^{L}\eta_i^\dagger\eta_i$. Using the notation $n_i = \eta_i^\dagger\eta_i$, H' in the diagonal basis is, thereby,

$$H' = -\frac{BL}{2} + \sum_{i=1}^{L} n_i\left(\lambda_i + B\right). \tag{C.5}$$

The next step is to calculate the so-called partition function Z, which is defined as

$$Z = Tr\left(\sum_{\{n_j\}} e^{-\frac{1}{T}H'}\right), \tag{C.6}$$

where the set $\{n_j\}$ represents the j-th microstate of the system. Substituting Eq. C.5 in Eq. C.6 gives

$$Z = e^{\frac{BL}{2T}} \sum_{\{n_j\}} \exp\left[-\frac{1}{T}\sum_{i=1}^{L} n_i\left(\lambda_i + B\right)\right]. \tag{C.7}$$

The sum of exponents can be replaced with a product of exponentials. This product commutes with the sum over all microstates. Since the value of n_i is either one or zero, the expression for the partition function becomes

$$\begin{aligned} Z &= e^{\frac{BL}{2T}} \prod_{i=1}^{L}\left[e^{-\frac{1}{T}(\lambda_i+B)} + 1\right], \\ &= e^{\frac{BL}{2T}} \prod_{i=1}^{L} e^{-\frac{1}{2T}(\lambda_i+B)} \frac{2}{2}\left[e^{\frac{1}{2T}(\lambda_i+B)} + e^{-\frac{1}{2T}(\lambda_i+B)}\right], \\ &= e^{\frac{BL}{2T}} \prod_{i=1}^{L} e^{-\frac{1}{2T}(\lambda_i+B)} 2\cosh\left(\frac{\lambda_i + B}{2T}\right). \end{aligned} \tag{C.8}$$

The free energy F is given in terms of the partition function as

$$F = -T\ln\left(Z\right), \tag{C.9}$$

Thus, substituting Eq. C.8 in the equation above gives

$$F = -T\left\{\frac{BL}{2T} + \sum_{i=1}^{L}\left[\ln 2 - \frac{\lambda_i}{2T} - \frac{B}{2T} + \ln\cosh\left(\frac{\lambda_i + B}{2T}\right)\right]\right\}. \tag{C.10}$$

Noticing that the sum over all eigenvalues is zero and that the two terms with B cancel out, one can divide Eq. C.10 by L and find the free energy density

$$f = -T\left[\ln 2 + \frac{1}{L}\sum_{i=1}^{L}\ln\cosh\left(\frac{\lambda_i + B}{2T}\right)\right]. \tag{C.11}$$

Therefore, with Eq. C.11 the calculation of the specific heat and the magnetic susceptibility is straightforward. The first derivative with respect to the temperature is

$$\frac{\partial f}{\partial T} = -\ln 2 - \frac{1}{L}\sum_{i=1}^{L}\ln\cosh\left(\frac{\lambda_i}{2T}\right) + \frac{1}{2LT}\sum_{i=1}^{L}\lambda_i\tanh\left(\frac{\lambda_i}{2T}\right), \tag{C.12}$$

using $B = 0$. The second derivative is

$$\frac{\partial^2 f}{\partial T^2} = -\frac{1}{4LT^3}\sum_{i=1}^{L}\lambda_i^2\cosh^{-2}\left(\frac{\lambda_i}{2T}\right). \tag{C.13}$$

Substituting Eq. C.13 in Eq. C.1 gives

$$C = \frac{1}{2LT^2} \sum_{i=1}^{\frac{L}{2}} \lambda_i^2 \cosh^{-2}\left(\frac{\lambda_i}{2T}\right), \tag{C.14}$$

since the spectrum is symmetric and $\cosh(x) = \cosh(-x)$. Similarly, one can take the second derivative of Eq. C.11 and find that

$$\chi = \frac{1}{2LT} \sum_{i=1}^{\frac{L}{2}} \cosh^{-2}\left(\frac{\lambda_i}{2T}\right). \tag{C.15}$$

APPENDIX D – Spin-spin and dimer-dimer correlation functions

This appendix provides a detailed deduction of the expressions for the correlation functions.

From the definition in Eq. 3.8, one can apply Eq. 2.10 and find that the z-component spin-spin correlation function in terms of fermionic operators is

$$\begin{aligned} G^z(r) &= \left\langle \left(c_i^\dagger c_i - \frac{1}{2}\right)\left(c_j^\dagger c_j - \frac{1}{2}\right)\right\rangle, \\ &= \left\langle c_i^\dagger c_i c_j^\dagger c_j\right\rangle - \frac{1}{4}, \end{aligned} \tag{D.1}$$

since $\left\langle c_i^\dagger c_i\right\rangle = 1/2, \forall\, i$. Using Wick's theorem (27, 69) one can show that the expectation value of the product of four fermionic operators (namely A, B, C and D) is

$$\langle ABCD\rangle = \langle AB\rangle\langle CD\rangle - \langle AC\rangle\langle BD\rangle + \langle AD\rangle\langle BC\rangle, \tag{D.2}$$

Thus,

$$\begin{aligned} \left\langle c_i^\dagger c_i c_j^\dagger c_j\right\rangle &= \left\langle c_i^\dagger c_i\right\rangle\left\langle c_j^\dagger c_j\right\rangle - \left\langle c_i^\dagger c_j^\dagger\right\rangle\langle c_i c_j\rangle + \left\langle c_i^\dagger c_j\right\rangle\left\langle c_i c_j^\dagger\right\rangle, \\ &= \left\langle c_i^\dagger c_j\right\rangle\left\langle c_i c_j^\dagger\right\rangle + \frac{1}{4}, \\ &= -\left\langle c_i^\dagger c_j\right\rangle^2 + \frac{1}{4}, \end{aligned} \tag{D.3}$$

since $\left\langle c_i^\dagger c_j^\dagger\right\rangle = \langle c_i c_j\rangle = 0$ and $\left\langle c_i c_j^\dagger\right\rangle = -\left\langle c_j^\dagger c_i\right\rangle = -\left\langle c_i^\dagger c_j\right\rangle$. Hence, substituting Eq. D.3 in Eq. D.1 gives

$$\begin{aligned} G^z(r) &= -\left\langle c_i^\dagger c_j\right\rangle^2, \\ &= -\left(\sum_{k=1}^{\frac{L}{2}} v_{ik} v_{jk}\right)^2. \end{aligned} \tag{D.4}$$

The approach to find the expression for $G^x(r)$ is similar. Using that $S_i^x = \left(S_i^+ + S_i^-\right)/2$ one finds

$$\begin{aligned} G^x(r) &= \frac{1}{4}\left\langle \left(S_i^+ + S_i^-\right)\left(S_j^+ + S_j^-\right)\right\rangle, \\ &= \frac{1}{4}\left\langle S_i^+ S_j^+ + S_i^+ S_j^- + S_i^- S_j^+ + S_i^- S_j^-\right\rangle. \end{aligned} \tag{D.5}$$

Substituting in the relation above the inverse of Eq. 2.6 and Eq. 2.7, i.e.

$$S_i^+ = c_i^\dagger e^{i\pi\phi_i}, \qquad S_i^- = e^{-i\pi\phi_i} c_i, \tag{D.6}$$

where $\phi_i = \sum_{k=1}^{i-1} c_k^\dagger c_k$, gives

$$G^x(r) = \frac{1}{4}\left\langle c_i^\dagger e^{i\pi\phi_i} c_j^\dagger e^{i\pi\phi_j} + c_i^\dagger e^{i\pi\phi_i} e^{-i\pi\phi_j} c_j + e^{-i\pi\phi_i} c_i c_j^\dagger e^{i\pi\phi_j} + e^{-i\pi\phi_i} c_i e^{-i\pi\phi_j} c_j \right\rangle. \tag{D.7}$$

It is useful here to expand the exponential as a Taylor series and verify that

$$\begin{aligned} \exp\left(\pm i\pi c_i^\dagger c_i\right) &= \sum_{j=0}^{\infty} \frac{(\pm i\pi)^j}{j!} \left(c_i^\dagger c_i\right)^j, \\ &= 1 + c_i^\dagger c_i \left(e^{\pm i\pi} - 1\right), \\ &= 1 - 2c_i^\dagger c_i, \end{aligned} \tag{D.8}$$

since $\left(c_i^\dagger c_i\right)^j = c_i^\dagger c_i, \forall\, j > 0$. Therefore, the exponential products in Eq. D.7 can be rewritten as

$$\begin{aligned} e^{\pm i\pi\phi_i} e^{\pm i\pi\phi_j} &= \left[\prod_{k=1}^{i-1} \left(1 - 2c_k^\dagger c_k\right)\right] \left[\prod_{m=1}^{j-1} \left(1 - 2c_m^\dagger c_m\right)\right], \\ &= \prod_{k=i}^{j-1} \left(1 - 2c_k^\dagger c_k\right), \end{aligned} \tag{D.9}$$

since $\left(1 - 2c_i^\dagger c_i\right)^2 = 1$. Thus,

$$\begin{aligned} G^x(r) &= \frac{1}{4}\left\langle \left(c_i^\dagger c_j^\dagger + c_i^\dagger c_j + c_i c_j^\dagger + c_i c_j\right) \prod_{k=i}^{j-1} \left(1 - 2c_k^\dagger c_k\right) \right\rangle, \\ &= \frac{1}{4}\left\langle \left(c_i^\dagger + c_i\right)\left(1 - 2c_i^\dagger c_i\right) \left[\prod_{k=i+1}^{j-1} \left(1 - 2c_k^\dagger c_k\right)\right] \left(c_j^\dagger + c_j\right) \right\rangle, \\ &= \frac{1}{4}\left\langle \left(c_i^\dagger - c_i\right) \left[\prod_{k=i+1}^{j-1} \left(c_k^\dagger + c_k\right)\left(c_k^\dagger - c_k\right)\right] \left(c_j^\dagger + c_j\right) \right\rangle. \end{aligned} \tag{D.10}$$

Defining new operators $A_i \equiv \left(c_i^\dagger + c_i\right)$ and $B_i \equiv \left(c_i^\dagger - c_i\right)$ and substituting them in the equation above gives

$$G^x(r) = \frac{1}{4}\left\langle B_i A_{i+1} B_{i+1} \ldots A_{j-1} B_{j-1} A_j \right\rangle. \tag{D.11}$$

Once again one can use Wick's theorem to write the product of $2(i + j - 1)$ operators as a sum of the product of pairs. Notice, though, that some of the pairs are equal to zero by definition. For instance,

$$\langle A_i A_j \rangle = -\langle B_i B_j \rangle = \delta_{i,j}, \tag{D.12}$$

which is always equal to zero for Eq. D.11, since no index is repeated. Conversely, the pairs $\langle B_i A_j \rangle = -\langle A_j B_i \rangle$ are given by

$$\begin{aligned} \langle B_i A_j \rangle &= \left\langle \left(c_i^\dagger - c_i\right)\left(c_j^\dagger + c_j\right) \right\rangle, \\ &= \left\langle c_i^\dagger c_j \right\rangle - \left\langle c_i c_j^\dagger \right\rangle, \\ &= 2\left\langle c_i^\dagger c_j \right\rangle - \delta_{i,j}. \end{aligned} \tag{D.13}$$

Hence one can write the product of operators in Eq. D.11 as the determinant of the matrix $\mathcal{G}(r)$ which has entries $\mathcal{G}_{i,j} = \langle B_i A_j \rangle$ (70), i.e.

$$\mathcal{G}(r) = \begin{vmatrix} 2\left\langle c_i^\dagger c_{i+1} \right\rangle & 0 & 2\left\langle c_i^\dagger c_{i+3} \right\rangle & \cdots & 2\left\langle c_i^\dagger c_j \right\rangle \\ 0 & 2\left\langle c_{i+1}^\dagger c_{i+2} \right\rangle & 0 & \cdots & 2\left\langle c_{i+1}^\dagger c_j \right\rangle \\ 2\left\langle c_i^\dagger c_{i+3} \right\rangle & 0 & 2\left\langle c_{i+2}^\dagger c_{i+3} \right\rangle & \cdots & \\ \vdots & \vdots & \vdots & \ddots & \vdots \\ 2\left\langle c_i^\dagger c_j \right\rangle & & \cdots & 0 & 2\left\langle c_{j-1}^\dagger c_j \right\rangle \end{vmatrix}. \tag{D.14}$$

The x-component spin-spin correlation function is, thereby,

$$G^x(r) = \frac{1}{4}\det\left(\mathcal{G}(r)\right). \tag{D.15}$$

Lastly, the dimer-dimer correlation function $G^{dd}(r)$. The first step is to insert Eq. 3.11 in Eq. 3.13, which yields

$$\begin{aligned} G^{dd}(r) &= \left\langle \left(-S_{2i-1}^x S_{2i}^x - S_{2i-1}^y S_{2i}^y + S_{2i}^x S_{2i+1}^x + S_{2i}^y S_{2i+1}^y\right) \right. \\ &\times \left. \left(-S_{2j-1}^x S_{2j}^x - S_{2j-1}^y S_{2j}^y + S_{2j}^x S_{2j+1}^x + S_{2j}^y S_{2j+1}^y\right) \right\rangle \\ &- \left\langle \left(-S_{2i-1}^x S_{2i}^x - S_{2i-1}^y S_{2i}^y + S_{2i}^x S_{2i+1}^x + S_{2i}^y S_{2i+1}^y\right) \right\rangle \\ &\times \left\langle \left(-S_{2j-1}^x S_{2j}^x - S_{2j-1}^y S_{2j}^y + S_{2j}^x S_{2j+1}^x + S_{2j}^y S_{2j+1}^y\right) \right\rangle \end{aligned} \tag{D.16}$$

For simplicity, it is considered the following substitution: $2i-1 \to i$, $2i \to j$, $2i+1 \to k$, $2j-1 \to l$, $2j \to m$, $2j+1 \to n$.

Notice that the distance between pairs of spin operators is always one. Thus, according to Eq. D.11 one can write

$$S_i^x S_j^x = \frac{1}{4} B_i A_j. \tag{D.17}$$

Similarly, for the y-direction one can find that

$$S_i^y S_j^y = \frac{1}{4} B_j A_i. \tag{D.18}$$

Therefore, $G^{dd}(r)$ can be written as

$$\begin{aligned} G^{dd}(r) &= \frac{1}{16}\left(\langle B_i A_j B_l A_m\rangle + \langle B_i A_j B_m A_l\rangle + \langle B_j A_i B_l A_m\rangle + \langle B_j A_i B_m A_l\rangle - \langle B_i A_j B_m A_n\rangle\right. \\ &- \langle B_i A_j B_n A_m\rangle - \langle B_j A_i B_m A_n\rangle - \langle B_j A_i B_n A_m\rangle - \langle B_j A_k B_l A_m\rangle - \langle B_j A_k B_m A_l\rangle \\ &- \langle B_k A_j B_l A_m\rangle - \langle B_k A_j B_m A_l\rangle + \langle B_j A_k B_m A_n\rangle + \langle B_j A_k B_n A_m\rangle + \langle B_k A_j B_m A_n\rangle \\ &+ \langle B_k A_j B_n A_m\rangle - 4\langle B_i A_j\rangle\langle B_l A_m\rangle + 4\langle B_i A_j\rangle\langle B_m A_n\rangle + 4\langle B_j A_k\rangle\langle B_l A_m\rangle \\ &- \left. 4\langle B_j A_k\rangle\langle B_m A_n\rangle\right). \end{aligned} \tag{D.19}$$

Using Eq. D.2 and that $\langle B_i A_j\rangle = 0$ for $|j-i|$ even, one can simplify the expression above until it reads

$$G^{dd}(r) = \frac{1}{8}\left(\langle B_i A_m\rangle - \langle B_k A_m\rangle\right)\left(\langle B_j A_n\rangle - \langle B_j A_l\rangle\right). \tag{D.20}$$

Retrieving the original indexes and using Eq. D.13 gives

$$G^{dd}(r) = \frac{1}{2}\left(\left\langle c^{\dagger}_{2i-1}c_{2j}\right\rangle - \left\langle c^{\dagger}_{2i+1}c_{2j}\right\rangle\right)\left(\left\langle c^{\dagger}_{2i}c_{2j+1}\right\rangle - \left\langle c^{\dagger}_{2i}c_{2j-1}\right\rangle\right). \tag{D.21}$$

APPENDIX E – Fitting method of the entanglement entropy scaling with subleading terms

This appendix explains the fitting procedure of the entanglement entropy with a subleading correction to the scaling (Eq. 4.11).

The least-squares method consists in determining the set of parameters $\boldsymbol{a}$ that minimize the following quantity

$$Q = \sum_{i=1}^{N} \left[y_i - f\left(x_i, \boldsymbol{a}\right) \right]^2 , \tag{E.1}$$

where N is the number of points, y_i are the measured data and $f\left(x_i, \boldsymbol{a}\right)$ is the theoretical scaling function. For the entanglement entropy, $N = L/2$ and

$$f\left(x_i, \boldsymbol{a}\right) = a_0 + a_1 h_1\left(x\right) + a_2 h_2\left(x\right), \tag{E.2}$$

where x is the subsystem size and

$$h_1\left(x\right) = \ln\left[\frac{L}{\pi} \sin\left(\frac{\pi x}{L} \right) \right], \tag{E.3}$$

$$h_2\left(x\right) = \frac{\left(-1\right)^x}{\left[\frac{L}{\pi} \sin\left(\frac{\pi x}{L} \right) \right]^{a_3}}. \tag{E.4}$$

Taking the gradient of Q with respect to $\boldsymbol{a}$ and setting it equal to zero gives the following system of equations

$$\sum_i a_0 + a_1 \sum_i h_1\left(x_i\right) + a_2 \sum_i h_2\left(x_i\right) = \sum_i y_i, \tag{E.5}$$

$$a_0 \sum_i h_1\left(x_i\right) + a_1 \sum_i \left[h_1\left(x_i\right)\right]^2 + a_2 \sum_i h_2\left(x_i\right) h_1\left(x_i\right) = \sum_i y_i h_1\left(x_i\right), \tag{E.6}$$

$$a_0 \sum_i h_2\left(x_i\right) + a_1 \sum_i h_2\left(x_i\right) h_1\left(x_i\right) + a_2 \sum_i \left[h_2\left(x_i\right)\right]^2 = \sum_i y_i h_2\left(x_i\right), \tag{E.7}$$

$$a_0 \sum_i h_2\left(x_i\right) h_1\left(x_i\right) + a_1 \sum_i h_2\left(x_i\right) \left[h_1\left(x_i\right)\right]^2 + a_2 \sum_i \left[h_2\left(x_i\right)\right]^2 h_1\left(x_i\right) = \sum_i y_i h_2\left(x_i\right) h_1\left(x_i\right). \tag{E.8}$$

Notice that all the equations above are nonlinear with respect to a_3 and linear with respect to the other parameters. The linear parameters can be calculated exactly, after determining

the nonlinear one. To determine a_3 one can apply Newton's method, which is an iterative method represented as the following

$$a_3^{(k+1)} = a_3^{(k)} - \frac{g\left(a_3^{(k)}\right)}{g'\left(a_3^{(k)}\right)}, \tag{E.9}$$

where k is the k-th step of the iteration. It is considered the function $g\left(a_3^{(k)}\right)$ as the difference between the left and right-hand side of Eq. E.8, and the derivative $g'\left(a_3^{(k)}\right)$ is calculated with respect to a_3.

The objective is to plot the fitting parameters $\boldsymbol{a}$ as a function of the parameter n of the Rényi entanglement entropy. The best results were obtained by calculating a_3 for $n = 10$ first, using as initial guess the clean chain value $a_3^{(0)} = 1/5$. The iterative method stops whenever $\left|g\left(a_3^{(k)}\right)\right| \leq 10^{-5}$, or when the maximum of 10^3 iterations is reached. If an iteration yields an unreliable value of a_3, i.e. $a_3 < 0$ or $a_3 > 5$, the next step returns to the initial guess $a_3^{(0)}$. Substituting the final value of a_3 in Eq. E.5, Eq. E.6 and Eq. E.7 gives the other parameters. This procedure is repeated for every value of n, which is varied from $n = 10$ to $n = 1$ with a step of 0.1. However, for $n < 10$ the initial guess $a_3^{(0)}$ corresponds to the final value of a_3 computed for the previous n.